UNIVERSITÀ DEGLI STUDI DI ROMA

"TOR VERGATA"

FACOLTÁ DI SCIENZE MATEMATICHE FISICHE E NATURALI

DOTTORATO DI RICERCA IN

SCIENZE CHIMICHE

CICLO XXII

Preparation and Characterization of Hybrid Csp^2 - Csp^3 Materials and Nanodiamond-based Systems

Valeria Guglielmotti

A.A. 2009/2010

Tutor: Prof.ssa Maria Letizia Terranova

Coordinatore: Prof. Bruno Crociani

La mente
è come un paracadute
funziona
solo se si apre

"A. Einstein"

Contents

Background and motivation

Nowadays the research for nanostructured materials is a natural consequence of technological evolution. In fact, unexpected material properties arising from the particles reduction down to the nanometer scale allows a completely different approach into a wide set of applications.

Carbon allotropes like diamond and nanotubes (CNTs), despite having different carbon-carbon bonds, are the toughest and strongest materials, respectively. The exceptional properties of carbon nanotubes such as high tensile strength, excellent radial elastic deformability and extreme toughness have paved way for their use in next generation composite materials.

Furthermore, CNTs are used for different applications due to their exotic electronic and mechanical properties, among which the semiconductor/metallic behaviour or the extreme elastic modulus.

At the same time diamond is also distinguished by its extreme hardness, high thermal conductivity, low thermal expansion and self-friction coefficients. More recently a special class of diamond structure at the nanoscale has been discovered: this material is often called 'ultra-nanocrystalline' diamond with characteristic size of the basic diamond constituents encompassing the range of just few nanometers.

Particles with typical sizes of 4-5 nm, often called in the literature "ultradispersed diamond" (UDD) or "detonation nanodiamond" (DND), were produced by detonation of carbon-containing explosives in the URSS in the 1960s. But nowadays this material has gained a world-wide attention due to its inexpensive large scale synthesis based on the detonation, small primary particle size (few nanometers) with narrow size distribution, surface functionalization including bioconjugation, as well as high biocompatibility.

Among the several applications of this novel material, it should be mentioned its use in pretreatment processes of substrates in the diamond synthesis by Chemical Vapor Deposition (CVD). In fact the quality of polycrystalline diamond films depends strongly on the initial nucleation density (*'seeding'*) and subsequently on the size and distribution

of the seeds. So nanodiamond particles represent an excellent ideal seeding solution to the thinking of many researchers.

The ability to produce diamond specimens with complex three-dimensional shapes is at present a very challenging requirement of any diamond-based technology. In a first part of this thesis work, results obtained by using aqueous nanodiamond colloids to produce 'shaped' polycrystalline diamond films with modified hot filament CVD apparatus (Patent M. L. Terranova, M. Rossi, V. Sessa, S. Piccirillo MI98A001159 extended to PCT/E999/0347) are reported and discussed. This study is a part of ongoing effort to improve the seeding technique, with the focus on the seeding solution itself.

It is well-known that CVD-produced diamond materials span a continuum in grain sizes, morphologies, defect structures and concentrations. As a consequence their properties change from high quality, as in the case of nearly perfect single crystals, to polycrystalline materials where the grain size can vary continuously from barely displaying evidence of crystallinity to mm-sized grains [1].

In this contest, with the aim to produce diamond films with improved quality and properties, we have exploited the experimental parameters normally used for conventional CVD diamond growth in the synthesis of polycrystalline diamond films onto an innovative substrate constituted by a superconducting material like niobium nitride (NbN).

The focal poin has been the study of the catalytic effect induced by NbN during the CVD growth compared to the most used Si. Furthermore a patterned substrate ('multi-finger device') has been also used for the diamond growth in order to study the possibility of producing diamond-based device at the micrometric scale. The structural and morphological properties of the prepared samples have been characterized and discussed in the first part of this work.

More recently, an important task is represented by the study of the benefits obtained by the integration of different nanosized carbon forms for the realization of novel hybrid Csp^2-Csp^3 systems.

These systems, composed by CNT and diamond, can be expected to have unique mechanical properties, excellent electrical and thermal conductivities and field emission characteristics comparable to or better than pure diamond and CNTs.

Diamond/CNT hybrids may thus find applications in various fields such as wear-resistant coatings, thermal management of integrated circuits (ICs), field emission devices and electrical field shielding in MEMS and microelectronics [2].

As consequence, more research in this field is mandatory in what concerns the synthesis

itself and also the properties characterization of this new class of materials.
In literature there are several works involving the integration of these two carbon forms, as for example the phase transformation of CNTs into diamond [3] and the growth of nanosized diamond on CNTs [4].

Other recent studies have been done concerning the definition of the processing parameter window for the simultaneous growth of these two materials [5]. For example using the typical growth conditions for diamond by hot filament CVD (HFCVD), Yang *et al.* [5] grew simultaneously, yet separately, CNTs and diamond. The first ones were deposited on a substrate region coated with a nickel catalyst whereas the second in a previously diamond powder scratched zone. However, a real connection between the two forms could not be observed.

Starting from this research, an important part of the thesis work was focused on one-step synthesis, by means of a Chemical Vapor Deposition Technique, of CNTs/nanodiamond systems and their structural, morphological and functional characterizations.

In a previous work [4], our group employing a modified HFCVD set-up capable of delivering nanocarbon particles to the reaction region, used Si samples pre-coated with submicron Fe clusters to obtain nanocrystalline diamond coated bundles of CNTs. In this study we exploit the experimental parameters usually optimized for CNTs or diamond growth by following a new synthesis process.

In this contest we have explored another preparation route of hybrid CNT/nanodiamond structures, suitable to be scaled up and adapted to the requirements of electronic industries. The preparation of deposits formed by CNT arrays coated by nanodiamond grains, using an one step chemical vapour deposition approach, has been optimized and the results obtained are presented and discussed.

1 Diamond

Diamonds were prized for their scarcity for centuries, and they remain a symbol of wealth and prestige to this day. Apart from their appeal as gemstones, diamonds have remarkable physical properties.

Diamond is the most appealing allotrope of carbon. It is formed by sp^3, tetrahedrally bonded carbon atoms, so that, in its most common crystalline structure, a sphalerite - like crystalline structure is formed. A glance at any handbook of material data properties will prove that diamond is almost always the biggest and the best.

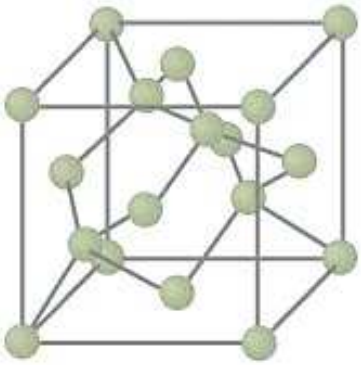

Figure 1.1: Crystal structure of cubic diamond

Among other properties, diamond is the hardest known material, it has the highest thermal conductivity at RT, it is transparent over a very wide wavelength range, it is the stiffest material and the least compressible and it is inert to most chemical reagents. With such a wide range of exceptional properties, it is not surprising that diamond has sometimes been referred to as the ultimate engineering materials. The most important properties are the following:

- Extreme mechanical hardness (ca. 90 GPa) and wear resistance

- Highest bulk modulus ($1.2 \cdot 10^{12}\mathrm{N} \cdot \mathrm{m}^{-2}$)
- Lowest compressibility ($8.3 \cdot 10^{-13}\ \mathrm{m}^2\mathrm{N}^{-1}$)
- Highest r.t. thermal conductivity ($2 \cdot 10^{3}\mathrm{W\ m}^{-1}\mathrm{K}^{-1}$)
- Very low thermal expansion coefficient at RT ($1 \cdot 10^{-6}\mathrm{K}$)
- Broad optical frequency from far UV to far IR
- Highest sound propagation velocity (17.5 Km/s)
- High electrical resistance (RT resistivity ca. 10^{13} Ωcm)
- Very resistant to chemical corrosion
- Biologically compatible

Unfortunately, in the past it has proved very difficult to exploit these properties, due both to the cost and scarcity of large natural diamonds, and the fact that diamond was only available in the form of stones or grit.

In the early 1990s, the rapid progress in this field leads to speculation that diamond would become the next-generation ideal semiconductor and spark a new "diamond age" for electronics and mechanical components.

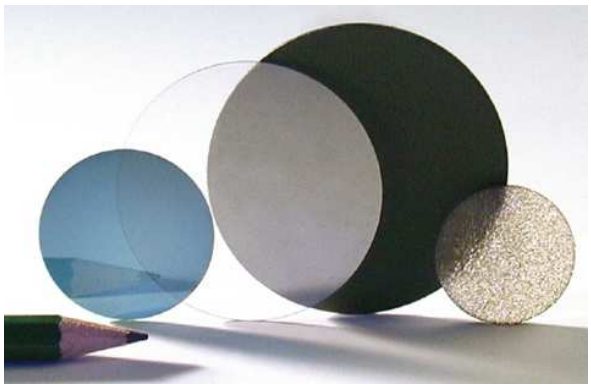

Figure 1.2: Policrystalline diamond based disk

In particular, about the electronic properties of diamond the scientific community usually defines this carbon allotrope as an electrical insulator or, depending on the point

of view, a wide bandgap semiconductor. In a bulk, single crystal, pure diamond, the conduction band minimum is about 5.5 eV apart from the valence band maximum. The energy difference between the vacuum level and the conduction band minimum is called the electron affinity and labelled as χ: it has been shown that pure diamond has an electron affinity of about 0.4eV while a hydrogen terminated diamond may have a negative electron affinity (NEA) [6]. It means that if an electron reached the conduction band minimum, it would be emitted without overcoming a barrier (ballistic emission).

For a diamond film synthesized by Hot Filament Chemical Vapor Deposition (HFCVD), the surface will automatically be terminated with hydrogen. Cui *et al.* attributed the NEA to the surface dipole formed by C^- - H^+ bond at the surface [7]. The length of the dipole was estimated to be 1.1 Å [7] and an electron will see a potential drop in the dipole layer as large as 1.65 eV, which is equivalent -according to Cui, who attributes to NEA for (111) surface the value -1.27 eV- to the change in χ.

The idea of getting diamond more conductive has always been an appealing task: both p-type and n-type doping have been persecuted. P-type doped diamond occurs naturally, being supplied by a certain quantity of boron atoms. Its poor abundance and reproducibility in electronic properties make it unused for the desired -electronic, optoelectronic- applications.

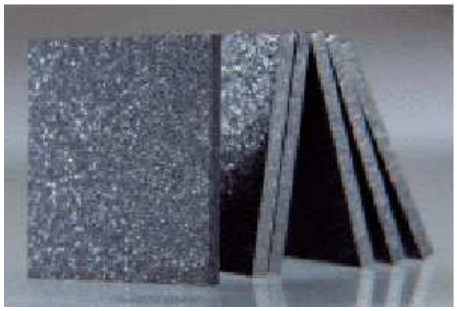

Figure 1.3: Electrically conductive polycrystalline CVD diamond plates

Diamond can be doped artificially by ion implantation but a further annealing step is needed to remove the structural damages due to the ion beam. Moreover, graphitization and amorphization may occur, what make the technique of relative usefulness.

CVD technique, where B-containing precursors or B_2H_6 are usually added to the gaseous mixture in the reactor, has proved so suitable for doping diamond that it is

nowadays of industrial application. However, it has been shown experimentally that the bandgap of intrinsic diamond begins to decrease with a concentration of B atoms larger than 10^{19}atoms/cm^3 [8]. For B concentration larger than 10^{20}atoms/cm^3 diamond shows a semimetal behaviour with a resistivity of 0.001Ω/cm (high doping levels are to be avoided if one needs a certain degree of crystallinity)[8].

N-type doping diamond is a more challenging task than p-type doping. The presence of a donor level near the conduction band minimum would make emission -whether field-induced or photostimulated- much easier; moreover, the availability of n-type diamond would pave the way to the realization of p-n junctions and therefore of a number of electronic devices.

The search for donors must involve atoms with the right features to fit in the diamond lattice; they are the alkaline metals such as Li and Na which can occupy interstitial sites, whereas V-group and VI group elements are destined to substitutional sites. Among these, the only guest atom which, so far, has given clear proof of doping diamond is P, inserted by the use of P-containing molecules (PH_3) in the CVD synthesis [9, 10].

Last but not least, structural defects such as vacancies, impurities (the most common of which is constituted by H), grain boundaries, sp^2 hybridized C atoms may lead to the formation of defect-induced bands endowed with a donor character: they may be responsible of electron hopping processes which generally enhance conductivity. This is the reason why, when studying the electron transport in a nominally doped diamond, it is really difficult to separate the donor contribution from the defect contribution.

1.1 Detonation Nanocrystalline Diamond

Nowadays materials scientists have at their disposal a convenient nanocarbon building block for further progress in nanotechnology. As shown in the previous paragraph, the appeal of diamond originates from two aspects: first, this material is incomparable among other semiconductor materials in the magnitude of its saturated carrier drift velocity in strong electric fields and the possibility of working at high temperatures and in corrosive media. Second, recent progress in CVD technologies has opened up real prospects in the production of diamond films with parameters approaching the requirements imposed by modern semiconductor electronics.

Thanks to the remarkable features both in the structure and in the physicochemical properties of detonation nanodiamond (DND), this new kind of carbon could be considered as a specific *nanocarbon material* with a large and increasing popularity with respect to the family of nanocarbon clusters, fullerenes, nanotubes, nanographite and onions [11].

More than 40 years ago, researchers in the USSR found that diamond nanoparticles were formed as a product of the detonation of carbon-based explosives [12]. For several reasons, including the confidential military secrets in place in the USSR and a lack of industrial interest in nanotechnology at the time, the application of this nanodiamond (ND) remained unreported and under-exploited until very recently.

At the moment, the recent progress in the nanotechnologies has produced more interest in nanodiamond, as it could be considered an elementary building block in the frame of carbon technologies.

The term *nanodiamond* (ND) refers, generally speaking, to several objects, namely nanodiamond crystals found embedded in meteorites, crystalline grains in polycrystalline diamond films and also as powders and suspensions prepared by detonation synthesis. The synthesis consist of a detonation in sealed stainless steel chamber in the absence of oxygen containing carbonaceous precursors (usually a 40/60 to 70/30 TNT/hexogen mixture)[13].
The pressures and temperatures reached at the shock wave front (P $\sim$ 20–30 GPa, T $\sim$ 3000–4000 Kelvin) are in the region of thermal stability of the diamond (if we consider the phase diagram of carbon fig 1.4).

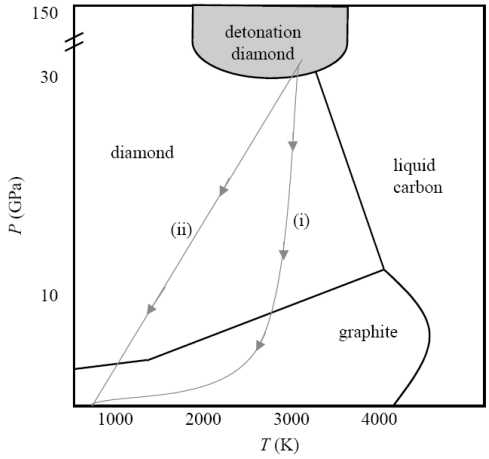

Figure 1.4: Phase diagram for carbon (adapted from [13]). i) Rapid decrease in P at high T lead to diamond-to-graphite transition. ii) Rapid cooling ensures diamond as the most stable phase

Generally, the detonation-assisted decomposition occurs in a non-oxidizing environment but the kinetics of the process is the predominant factor in the crystallization of the grains. Because of the P–T parameters, the synthesis passes through the region of kinetic diamond instability but after the detonation of the explosives, the temperature and pressure drop rapidly, falling in the region where diamond is thermodynamically unstable.

Theoretical calculations show that conditions for diamond stability during this process are only retained for a very short time (sub-microsecond) and are closely followed by conditions where graphite is the more stable phase.

To obtain diamond, it is therefore important to control the rate at which the system cools, i.e. faster cooling at relatively high pressure results in a higher diamond yield.

In fact if the temperature is still high enough to sustain a high mobility of the carbon atoms, the diamond–graphite reverse transition will be more probable than in the case where the transition to the region of thermodynamic stability of graphite takes place.

As consequence of this relationship between the rates of cooling and pressure drop, the as-synthesized material is characterized by the formation of C sp^2 as a thin coating onto the surface of diamond grains or as aggregates in the detonation carbon [14, 15], as illustrated in Fig. 1.5.

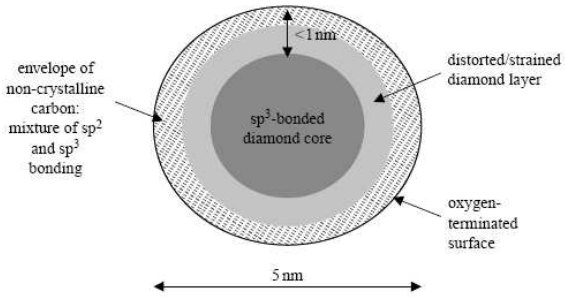

Figure 1.5: Schematic of a tentative model for a structure of 5 nm detonation ND (adapted from [15]. The figure is not drawn to scale)

After the synthesis process, several purification steps by means of mechanical and chemical methods are carried out on the material produced.

In particular acid purification at high temperatures is considered to be the best approach because it is able to remove most impurities, dissolving the metals and oxidizing at the same time the non-diamond carbon. Often the impurities present on the surface of the nanometric grains are functional groups and these are difficult to remove by wet chemistry.

Moreover, because of the high surface energy, the ultra nanometric material usually is inclined to form some agglomerates that ranges from few nanometres to one micron in size. In fact, this is the case of the suspension and the coalescence is the direct consequence of the high surface energy of the nanosized particles.

Under these characteristics, the characterization of nanodiamond particles is carried out with the aim to understand the average size of the nanodiamond clusters, the C sp^2/sp^3 ratio and the presence of impurities both in the diamond core and on the surface of the particles.

Nowadays, the scientific community involved in the study of this material had reached some important informations, as the crystal structure of the internal core of the particles, i.e. the real diamond lattice, and that each nanodiamond particle is coated by a shell constituted of different sp hybridized atoms.

At this aim, the typical diamond properties, i.e. the hardness, chemical stability, wide bandgap, the narrow size distribution of nanodiamond grains centred at 4–5 nm and the possibility to functionalize the surface, suggest the use of this material in several

application fields which range from mechanical applications to electronic ones, as field emitters [16].

Among these NDs have already shown that they could be used as ideal material in the *seeding* process usually used to produce diamond films by means of CVD techniques. In particular it should be stressed that the key step in the CVD technology of this kind of growth is the creation of a high concentration of *diamond nuclei* onto the substrate and also the increase of the nucleation rate during the synthesis.

Moreover the use of NDs for CVD technology can strongly influence the roughness of the surfaces of the as-produced films, inducing a decrease of roughness down to 1–3% and bringing to the development of a film growth technology on substrates which do not have any chemical affinity to carbon.

Finally the rich surface chemistry of ND, the absence of toxic impurities and small size make nanodiamonds a very convenient object for biomedical applications. Creation of specific surface sites on NDs for selective molecular attachment is considered a promising approach for their applications in nanofabrication, self-assembly,nanosensors, bioprobes, drug delivery, pigments, and so on.

1.2 HFCVD diamond synthesis

Although the standard enthalpies of diamond and graphite only differ by 2.9 kJ/mol, it is widely known that at room temperature and pressure a large activation barrier prevents interconversion between the two forms. Therefore, in order to synthesize diamond, researchers tried to look for the needed conditions where diamond is the more stable phase.

The knowledge of the conditions under which natural diamond is formed deep underground suggested that diamond could be synthesized by heating carbon under extreme pressures: as a consequence the so called high-pressure-high-temperature (HPHT) technique gained role.

This method produces single crystals ranging in size from nanometres to millimetres but what is required by most potential applications aiming to exploit the superlative diamond properties is often a thin film.

Rather than trying to duplicate nature's method to create it, diamond could conceivably be produced if carbon atoms could be added one-at-a-time to an initial template, in such a way that a tetrahedrally bonded carbon network results. The idea of the thermal decomposition of carbon containing gases under reduced pressures paved the way to the common Hot Filament Chemical Vapor Deposition technique (see fig 1.6).

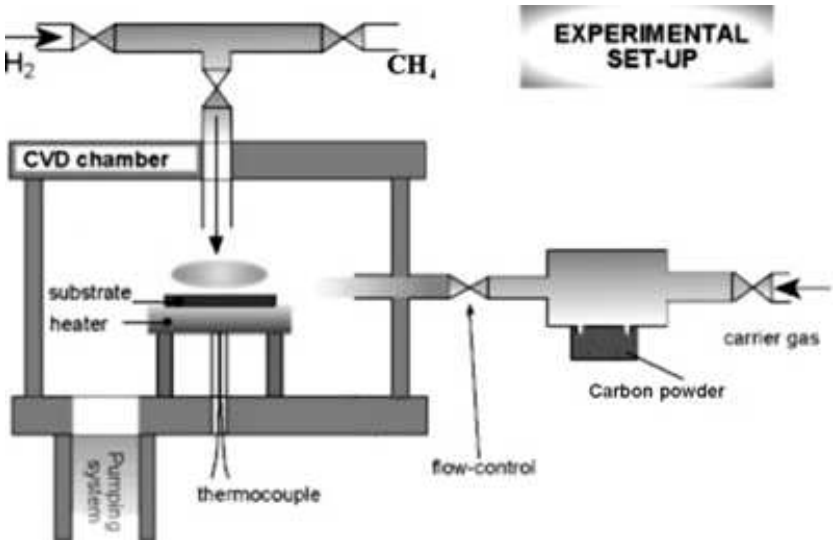

Figure 1.6: Scheme of the experimental set-up used in the HFCVD

By means of the only thermal decomposition, the growth onto the surface of a natural diamond crystal occurs, but the growth rate is really low, since graphite is co-deposited with diamond. A breakthrough came when it was discovered that the presence of hydrogen during the decomposition process leads to the preferential etching of graphite.

The first studies regarding the processes involved during the CVD synthesis can be attributed to Bachmann [17] which obtain the C-H-O compositional diagram (see Fig. 1.7) that bears his name. This diagram was elaborated after more over 70 deposition syntheses by using different reactors and several gas mixture.

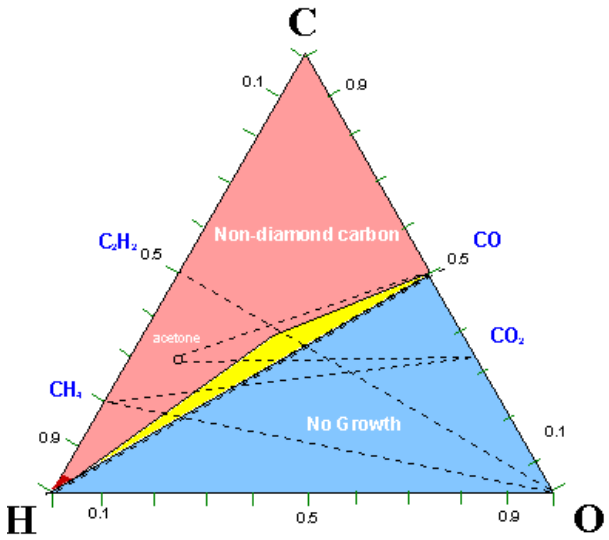

Figure 1.7: Bachmann diagram: the boundaries of the diamond growth domain in the triangular C-H-O gas composition

From these studies, some important information have been deduced. In particular, the diamond growth happens only in a little triangular area of the C-H-O composition, which is slightly above the CO tie-line, regardless from the type of apparatus gases adopted. This fundamental aspect suggests that the reaction between the gases is extremely rapid and also that it is the real responsible for the diamond growth.

Nowadays all processes have been optimized and it can be summarized that diamond growth normally requires a carbon containing precursor gas (usually CH_4) diluted in excess of hydrogen in a typical mixing ratio of 1% vol. Also, the temperature of the substrate is usually higher than 700°C. In a Hot Filament system, atomic hydrogen, produced heterogeneously by thermal decomposition of H_2 on the hot filament surface, is responsible of some main factors for the whole chemical system [18]:

1. Although the bulk of diamond is sp^3 bonded, at the surface there are effectively dangling bonds which need to be terminated in some way in order to prevent cross-linkage and subsequent reconstruction of the surface to graphite: this surface termination, during growth, is performed by hydrogen [19, 20].

2. Atomic hydrogen etches graphite carbon many times faster than diamond-like carbon.

3. Atomic hydrogen is an efficient scavenger of long-chain hydrocarbons thus preventing the build-up of polymers or large ring structures.

4. Atomic hydrogen, finally, reacts with neutral species such as CH_4 to create reactive radicals such as $CH_3^{\bullet}$ which can then attach to suitable surface sites, as depicted in the scheme of Fig. 1.8.

By the simple expedient of changing the growth conditions, diamond films can be deposited with properties ranging from almost graphitic to those of natural diamond. For example, the surface morphology of the film depends critically upon the various process conditions, especially the gas mixing ratio.

The growth rates along the different crystalline faces of diamond are various and depend on the temperature and composition of reaction gases; so it is possible to control the degree of the orientation of the diamond crystals, by adjusting the synthesis parameters.
The α parameter (as depicted in Fig. 1.9) allows to know the morphology of the crystalline deposit if some specific experimental conditions are satisfied [21].

In fact α is defined as the ratio between the growth rate (V) along the (100) and (111) direction respectively:
$\alpha = \sqrt{3}V(100)/V(111)$
and it can be equal to 1 for the single cubic crystal, 3 for the single octaedric crystal and a value ranging between 1 and 3 for crystal with a mixed crystallographic structure.

In the case of the polycrystalline films, the value of α is an index of the film texture. Moreover Menon *et al.* [22] have defined the range of the methane concentrations and the substrate temperature which leads to formation of the prevalent crystalline form of CVD diamond film.

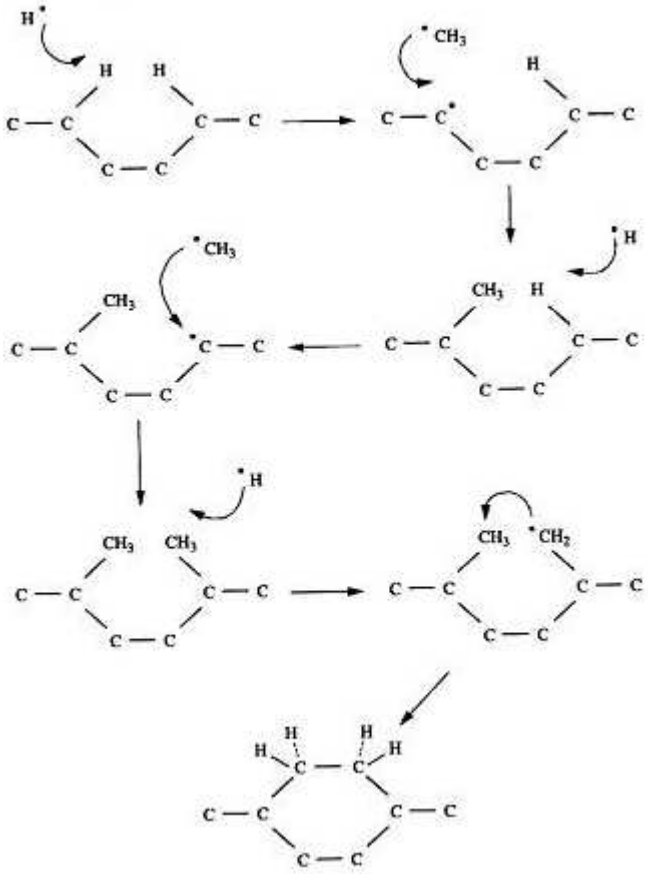

Figure 1.8: Scheme of the process of radical $CH_3^{\bullet}$ addition on the surface of 'diamond nuclei'

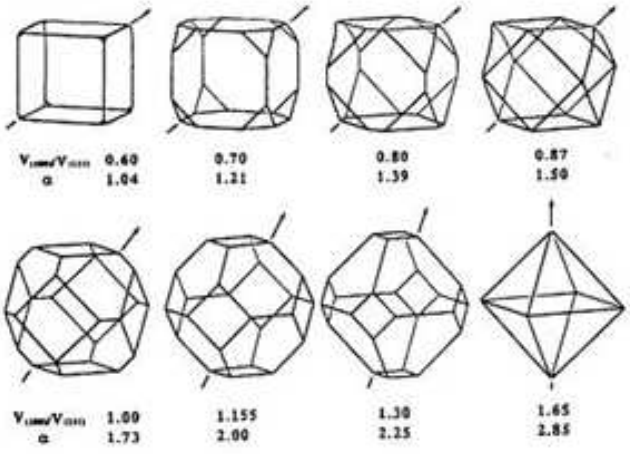

Figure 1.9: Crystalline structure of diamond: the arrow indicates the major direction of growth rate.

It is generally believed that the main growth species in standard diamond CVD is the CH_3 radical, which adds to the diamond surface following hydrogen abstraction by H atoms.

Thus, a high concentration of atomic H at the surface in addition to CH_3 radicals is a prerequisite for successful microcrystalline diamond deposition. By increasing the ratio of methane in the standard CH_4/H_2 gas mixture from 1% to 5%, the grain size of the films decreases, and eventually becomes of the order of hundreds down to tens of nm.

Such nanocrystalline diamond (NCD) films (often termed *cauliflower* or *ballas* diamond) are smoother than the microcrystalline ones, but have larger numbers of grain boundaries that contain substantial graphitic impurities. With further addition of CH_4 the films become graphitic.

Diamond has been nucleated and grown on diamond itself, plus a large variety of non-diamond substrates, including metals, semiconductors, insulators, graphite, and even fused glass, such as Mo, W, WC, ta, Cr, Co, Pt, Au, Al, Cu, Ni, Fe, stainless steel, NiAl, Ni_3Al, $FeSi_2$, Ti, TiN, TiC, Si, SiC, etc. Among these, Si wafer is probably the most commonly used substrate in diamond CVD.

Diamond nucleation on a substrate surface critically depends on the, chemical nature and surface condition of the deposition substrate. There is usually an initial incubation period in diamond CVD, i.e., a delay in nucleation before individual crystallites can be observed, followed by a delay in growth before these crystallites grow and coalesce together to form a continuous film.

Substrate pretreatment, scratching or seeding, is the most effective method for increasing surface nucleation density and decreasing the incubation method.

The simplest and useful method consists of mechanical scratching of the surface substrate with a solution containing diamond powders (with dimensions ranging from 10 nm to 10 microns) in a ultrasonic bath. On the other hand this method causes the damaging the surface in a not very reproducible way, it can be scarcely scaled up and it cannot be used in the case of substrate with micrometric dimensions as for the electronic devices.

Alternatively a bias-enhanced nucleation (BEN) method can be applied, which consist of applying a positive or negative voltage to the substrate, depending on the type of synthesis apparatus and experimental conditions adopted [23].

Seeding onto the substrate surface can be achieved with diamond powder or non-diamond powders as well as graphite flakes etc., or covering/coating substrate surface

with carbon clusters.

The effect of substrate surface pretreatment on diamond nucleation depends not only on the pretreatment methods but also on the type of substrates. Starting from these considerations, in this work of thesis an innovative approach for the method of 'seeding' by using the capability of surface-assisted self-assembling of detonation nanodiamond (DND) has been explore, in order to propose an innovative route to obtain 'shaped' CVD diamond films. Moreover the synthesis of polycrystalline diamond films onto a patterned substrate with superconductive properties, as niobium nitride (NbN), was investigated. The preliminary results obtained under predefinite experimental conditions are presented and discussed.

2 Carbon Nanotubes

Carbon nanotubes are a well-known form of carbon filament whose structure is usually described by the rolling up of one or more graphene sheets. In the first case we are in presence of a Single Wall Carbon Nanotube (SWCNT), in the second case of a Multi Wall Carbon Nanotube (MWCNT), as depicted in Fig. 2.1.

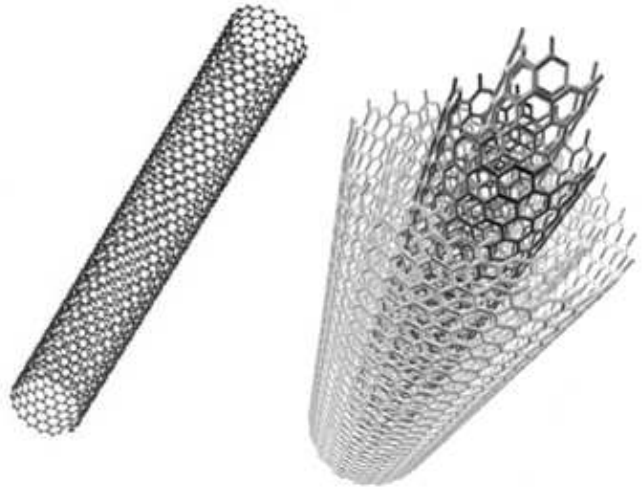

Figure 2.1: Examples of nanotubes structures

The most apparent feature of these structures is their high aspect ratio: their diameter ranges from 0.7 to 4-5 nm (SWCNT) and it reaches some tens of nanometres in the case of MWCNTs. Their length may reach the tens of microns. This ideal 1D structure has stimulated scientists to predict extraordinary physical properties.

The list of the unusual physical and chemical properties of carbon nanotubes is too long to be fully displayed here, so only a very brief report of them will be presented. Ref. [24] can be regarded as a good theoretical introduction to the world of carbon nanotubes.

In this contest it can be reminded, a number of different nanotube structures can be thought by varying the orientation of the 2D lattice of the graphene sheet with respect to the axis of the tube. Each structure is univocally described by a couple of integer indexes, named n and m, as illustrated in Fig. 2.2. They represent the two coefficients of the linear combination of graphite primitive vectors describing the so called chiral vectors.

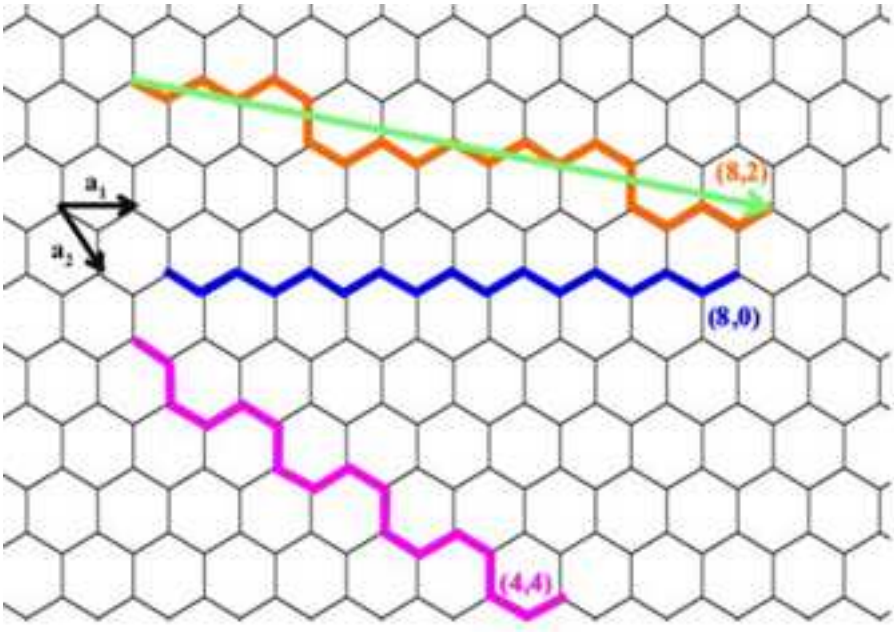

Figure 2.2: Graphene sheet and chiral vector for three single wall nanotubes defined as:(n,m) equal to (8,2), (8,0) and (4,4).

Each different couple of indexes leads, in the energy space, to a different electronic band arrangement; overall, the periodic boundary condition in the radial direction forces the density of states to a series of 1D Van Hove singularities.

The relative energy position of such singularities differs from structure to structure. The value of the bandgap varies as a function of the indexes, as well, thus making the electrical behaviour of the corresponding tubes ranging from semimetallic to semiconducting. In particular, when n - m is divisible by 3, the resulting nanotube is metallic; when n - m is not divisible by 3, the corresponding tube is semiconducting.

Ballistic conduction in certain conditions [24] has been predicted, thus making nanotubes ideal 1D conducting wires in the nanometric version of a number of electronic devices.

The strong planar carbon-carbon bond inherited from graphite is basically responsible for

- an incredibly high Young modulus
- low self-diffusivity even at high temperatures
- chemical inertness in relatively aggressive conditions
- low thermal resistance

Among the most popular applications of carbon nanotubes field emission, for example, is one of most suitable because of their listed features, together with the high aspect ratio of such structures.

In particular

- their aspect ratio directly determines their ability to amplify the applied electric field: this implies that CNT length should be maximized and the diameter minimized;
- their chemical inertness makes them robust against ion bombardment;
- they can face the high tensile stress due to the high applied field;
- because of their high thermal conductivity, they can sustain higher current than metallic emitters.

2.1 Carbon nanotube synthesis and characterization

The complete management of carbon nanotube synthesis represents the most challenging task in nanotube experimental research. A very brief review of the state of the art on synthesis will be provided here, mainly to list the key points.

First of all, up to now, there is no synthesis technique capable of growing a single type of CNT but abundance, purity, orientation and selected positioning onto predefinite areas of the substrates are appreciated features.

A number of different synthesis techniques have been set up. They can be roughly described as non equilibrium processes in extreme conditions i.e. high temperature, gas discharges. Carbon is provided as a solid -graphite- or as a gaseous hydrocarbon. SWCNT growth requires a metallic catalyst in form of clusters.
The three main categories of nanotube syntheses are:

- *Laser ablation.* The process consists of a laser-induced sublimation of a solid target with successive re-condensation of the material [25].

- *Arc discharge.* Two graphite electrodes in a low pressure of an inert gas are involved in an arc: evaporation from the cathode is followed by deposition of material on the anode [26].

- *Thermal activated, hot filament or plasma enhanced Chemical Vapor Deposition (CVD).* A carbonaceous gaseous phase is activated by heat/heated filament/plasma respectively; products of the decomposition of the gases and their consequent condensation on the substrate are the key points. [27].

The first two methods, which are really simply to be implemented and usually get effective results quite easily, produce abundant but non localized, dusty deposits.

Especially for arc-discharge the needed set-up is really inexpensive and the search for the optimal experimental conditions is not so difficult. The synthesis of SWCNTs generally requires a metal catalyst inserted as clusters into the solid carbon feedstock. Relative high quantity and high crystallinity of the product make arc-discharge the most widespread synthesis technique for nanotube mass production; as a consequence, the cheapest commercial carbon nanotubes are grown by arc discharge.

As in all kinds of nanotube synthesis techniques, a controlled adjustment of the experimental conditions may drive to a selected kind of product; in this regard, laser ablation

distinguished itself as the most promising technique to get a small spread of nanotube diameters.

The role of CVD techniques in the history of carbon material is crucial, therefore it requires a more deep discussion.

Over the years CVD methods have helped to unveil the fantastic diversity of carbon structures: a wide range of carbon structures can be grown (from diamond, diamond-like carbon to tetrahedral amorphous carbon - named ta-C - and graphitic nanostructures such as nanotubes) and then properties of the structures can be controlled over a large range.

CVD techniques require more complex and more expensive (especially plasma enhanced CVD) set-ups than arc-discharge or laser ablation set-ups, but produce localized deposits onto suitable substrates.

The process is generally catalysed by a metal pre-deposited onto the substrate as a thin film or simply by drop casting from a solution: the most popular catalyst is Nickel, but Cobalt and Iron are also widespread. Product quantity is generally very little, but selected positioning of the tubes is possible by exploiting a some kind of substrate selectivity due to direct/indirect action of the substrate itself on the catalytic activity of the metal or by simply patterning the catalyst as a thin film.

Orientation is generally achieved by means of an applied bias, so that CVD represents the most promising growth technique for several applications in the electronic field. Temperature is the limiting parameter in the choice of the substrate; for example, glass is generally not a suitable substrate for most of the CVD processes.

It is worthwhile stressing that, due to the different set-ups, different gaseous reactants, different substrates, different catalyst -both in nature and in physical phase- each synthesis process is unique: the as-grown material has in general its own self-organization, structure, and as a consequence physical and chemical properties.

The optimization of synthesis parameters, the full understanding of the growth steps and the achievement of a fully reproducibility of the process with prototypal CVD apparatuses are generally very hard tasks to be fulfilled, so that experimental research on nanotubes is often limited by impasses of the synthesis process.

Generally speaking, the challenge is threefold: to produce in a reproducible way "novel" carbon-based materials like nanotubes, to form self-supported or supported carbon-based thin films and finally to integrate directly carbon nanostructures into devices.

After synthesis, direct imaging of the morphology and of the structure of the sam-

ples can be achieved by -in order of increasing resolution- scanning electron microscopy (**SEM**), atomic force microscopy (**AFM**) and transmission electron microscopy (**TEM**). In Fig. 2.3 a typical TEM image of CNTs is shown.

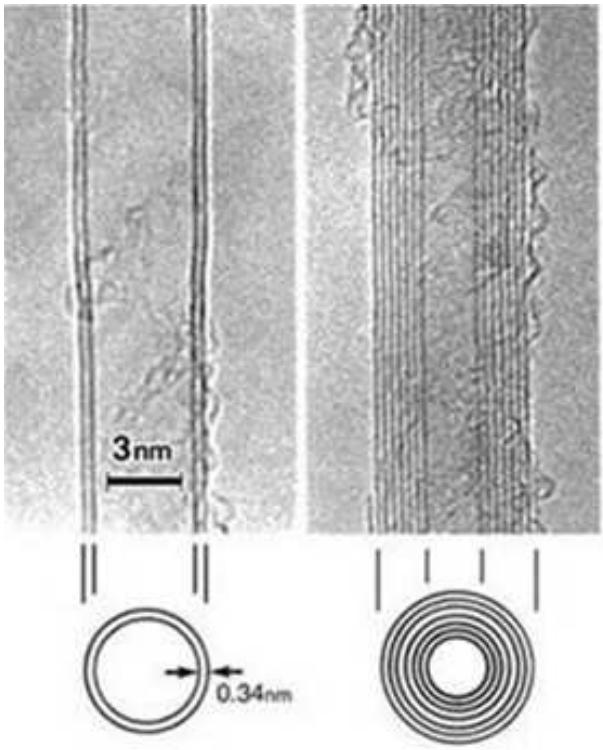

Figure 2.3: TEM images of multi wall carbon nanotubes

Diffraction techniques (X-ray diffraction and electron diffraction techniques, **RHEED** among the many available) have been used less extensively. Structural information are given by Raman spectroscopy in the tangential mode (1300 - 1700 cm^{-1}) and radial breathing mode region (100 - 300 cm^{-1}). Scanning tunnelling microscopy has been proved successful in confirming the unusual DOS in the energy space. In this work SEM, RHEED and Raman have been used to characterize the as-deposited material. Information about Raman characterization of CNT are provided in Ref. [24] while RHEED on CNTs is the subject of Ref. [28].

2.1.1 Synthesis of SWCNTs and MWCNTs with HFCVD apparatus at 'Tor Vergata' University

All the synthetic routes described briefly in the previous section utilize carbon precursors both in solid and gaseous phase in association with high temperature of reaction. Different structures can be obtained depending on the experimental paramteres such as temperature, working pressure, chemical species nearby the reaction site.

Even if from the theoretical point of view the formation of the rolled-up graphene sheet is favourite process, all the syntheses still adopted make use of metallic catalysts. Transition metals like Fe, Co, Ni and Y promote the nucleation and growth of SWCNTs.

In our lab, the CNTs growth by means of HFCVD technique has been optimized by using as catalyst Fe or Ni deposited on the substrate both by drop casting (a 10^{-5}M acetone solution) and by sputtering in form of thin films. Moreover by selecting the experimental conditions of synthesis and the nature of carbon precursors (methane or C nanopowders), deposits of both MWCNTs and SWCNTs respectively can be produced with our modified HFCVD set-up (Patent M. L. Terranova, M. Rossi, V. Sessa, S. Piccirillo MI98A001159 extended to PCT/E999/0347).

In the following list the typical experimental parameters usually adopted for the synthesis of CNTs are reported:

- filament temperature: 2100°C±10°C
- substrate temperature: 900°C±10°C
- woking pressure: 36 Torr
- typical filament/substrate distance: 10mm
- methane/hydrogen ratio flow varying according to the experiments
- pre-growing step followed by the synthesis

By using methane as C precursor in presence of metal catalysts, dense bundles of MWCNTs can be achieved with a synthesis of 30 minutes. Conversely when C nanopowders are used, the length of the synthesis is strongly reduced: in fact after 2 minutes we can already observe the presence of SWCNTs bundles.

The above conditions constitute the framework around which all synthesis experiments were carried out. Some parameters (filament/substrate distance, Ar flow, growth time) are indicated as variable in a well defined range.

With the aim to produce homogeneous and dense deposits, a particular care have been paid to the homogeneity of the catalyst dispersion on the substrate. During the sputtering deposition process of the catalyst a strong adhesion of the Fe or Ni film onto the Si substrate is guaranteed to resist to the aggressive synthesis conditions. Whatever the catalyst deposition process, a pre-growing step is needed.

For the substrate obtained by casting, since the active form of the catalyst is the metallic one, a chemical reduction of Fe^{3+}into Fe^{0} (or Ni^{2+} to Ni^{0}) must be performed; as for the sputtered layer, both a reduction of the superficial monolayers of oxide and a clustering of the film is required.

The exposure of the substrate to reactive hydrogen atmosphere constitutes an effective reduction treatment. Moreover, the aggressive nature of atomic H performs a some kind of bombardment, and thus of etching, leading to the clustering of the Fe or Ni film.

Moreover, CNT selective growth in predefinite areas of the substrates can be also achieved by using lithography techniques.

3 Csp^2 - Csp^3 hybrid materials

Hybrid materials represent one of the most fascinating developments in materials chemistry in recent years. The tremendous possibilities of combination of different properties in one material initiated an explosion of ideas about potential materials and related applications.

Recent technological breakthroughs and the desire for new functions generate an enormous demand for novel materials.

The term hybrid material, nowadays, is used for many different systems spanning a wide area of different materials: crystalline highly ordered coordination polymers, amorphous sol–gel compounds, materials with and without interactions between the inorganic and organic units.

All these categories define a novel material characterized by unusual properties which are a combination of the pristine ones belonging to the starting materials.

Recent strong scientific and technological interest in nanostructured carbon materials (*nanocarbons*) has been motivated by the different range of physical properties exhibited from these systems [5].
Moreover the increasing scale of device integration in solid-state technology coinciding with decreasing structure dimensions, requires the use of *nanomaterials* that can be fabricated into net shapes [29].

At the same time to realize the full potential of the new technologies, the material itself must survive under significantly severe environmental conditions and with this aim the family of *carbon nanostructures*, with outstanding mechanical, chemical, and thermal properties, is ideally suited to a wide range of innovative applications.

In particular carbon nanotubes (CNT), with sp^2 hybridization, show the exceptional properties of high tensile strength, excellent radial elastic deformability, extreme toughness and unique electronic transport properties and they have paved way for use in next generation composite materials [30].

Whereas diamond, with sp^3 hybridization and strong symmetric covalent bonding,

is by far the hardest known material. In addition, it has a low coefficient of thermal expansion and a high thermal conductivity, is chemically inert, offering a low friction coefficient and excellent wear resistance and biocompatibility.

It has been speculated that the synergistic combination of carbon nanotubes and nanocrystalline diamond could give rise to materials with novel properties that could be used advantageously in application that require a combination of good mechanical, thermal and electrical properties such as wear-resistant coatings, thermal management of integrated circuits (ICs), field emission devices and electrical field shielding.
These are only some applications for hybrid materials and there is a *plethora* of systems under development for future applications in various fields.

However, a synthesis pathway must be developed that would lead to the concurrent growth of different allotropes of carbon that are covalently bonded and organized at the nanometre-scale.

A number of works have been reported on development of hybrid materials comprising of diamond and CNT, namely the phase transformation of CNTs into diamond [2, 5, 31] and the growth of nanosized diamond on CNTs [30, 4].
Other recent studies have been done concerning the definition of the processing parameter window for the simultaneous growth of these two materials.

Various CVD techniques have been widely used to synthesize these two carbon materials. These two materials were usually synthesized separately under different conditions. To synthesize diamond, the vapour, usually composed of CH_4 (0.5–2.5 vol%) highly diluted in H_2, has to be activated by either generating a plasma or heating a filament up to high temperatures (2000–3000°C), while to synthesize carbon nanotubes, it is customary to use floating catalyst or catalyst thin films on substrates. So far, the growth of these two materials requires substrate temperatures typically between 700°C and 1100°C.

In particular, in this work we demonstrate that the simultaneous synthesis of nanocrystalline diamond and carbon nanotubes to form a covalently bonded hybrid material-a nanocomposite of diamond and CNTs- can be achieved.

4 Experimental: growth of Csp^2-Csp^3 hybrid systems and nanodiamond - based materials

4.1 HFCVD experimental apparatus

The synthesis apparatus utilized in this work consists of a conventional HFCVD reaction chamber connected to a powders flowing system (Patent M. L. Terranova, M. Rossi, V. Sessa, S. Piccirillo MI98A001159 extended to PCT/E999/0347).
A scheme of the apparatus is shown in Fig. 4.1.

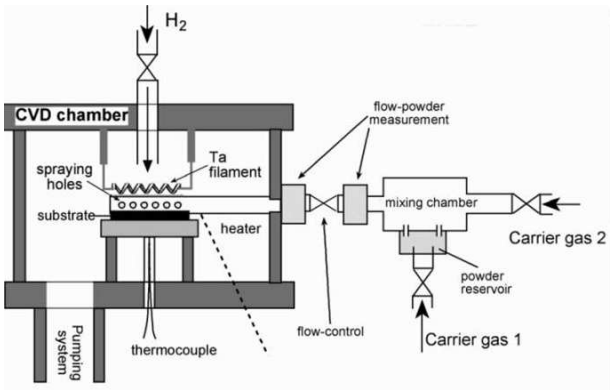

Figure 4.1: Scheme of our HFCVD apparatus

The reactor is made up by a 26 cm wide and 27,5 cm high cylindrical stainless steel vacuum chamber. It is connected in series to a rotative pump (Trivac 150 CVS), enabling a pressure of 10^{-3}Torr, and to a water-cooled turbomolecular pump (Turbovac 150 CVS), used to evacuate the reactor up to 10^{-5}Torr.

An ensemble of fluxmeters, valves and connections have been set up to exploit a number of different experimental conditions. Pressure inside the reactor is measured by means of three gauges, each of them purposely devoted to a different step of the process of evacuating the system and of establishing the desired conditions of pressure and atmosphere composition.

A 0,6 mm thick Ta wire (Goodfellow, with a purity of 99,85 %), rolled up into 20 coils to get a 1,5 mm long, rolled resistance, constitutes the Ta filament used to activate the gaseous phase. The choice of Ta is typical in HFCVD set-up: it is an inert, high-melting metal able to reach temperatures of more than 2000°C by Joule heating exposed to pressure of a few tens of Torr.

The sample holder is cut from a sintered 60 μm thick Mo slab (99,95% purity); its temperature is adjusted by means of a AC current generator and measured with a Pt/Pt-Ir thermocouple. As it is one of the key parameters in the synthesis process, the distance between filament and sample holder is monitored by an external measurement system (it is possible to mechanically intervene during growth, too).

The powders cell (as described in the previous section 2.1.1) is made up of a purposely realized glass reservoir connected to a gas flowing system. The used carrier gas is Ar. A metallic injector enables the gas-driven powders to reach the inside of the reactor; a Mo nozzle provides the powders delivery above the sample holder, just under the filament, in the area of reaction.

The powder flux can be mechanically oriented from about 10° to about 80° with respect to the plane of the sample holder while the hydrogen flux is always perpendicular to the sample holder.

4.2 Material characterization: experimental set-ups

Characterization of the as-grown material has been carried out by means of electron microscopy and some structural techniques: Raman spectroscopy, electron and x-ray diffraction.

4.2.1 Field emission gun scanning electron microscope (FEG-SEM)

The morphological characterization is carried out by means of a field emission gun-SEM (FEG-SEM). Our apparatus -Hitachi S-4000- enables a theoretical maximum magnification of 300000x.

Extraction voltage is about 0-6.5 kV, accelerating voltage ranging from 0.5 to 1 kV (variable in steps of 100V) and from 10 to 30 kV (variable in steps of 1 kV). A collector for secondary electrons is used. Digital image acquisition is carried out both by using, in low resolution, a common video card and by using a home-made high resolution image acquisition software (LabView).

4.2.2 Micro-Raman spectrometer

Raman spectroscopy is a powerful technique for the qualitative and quantitative analysis of organic and/or inorganic materials. Moreover is a non-destructive and non-invasive technique. This kind of analysis doesn't request any material preparation and it can be used to study material in solid, liquid and gaseous phase.

Typically, the sample is illuminated with a monocromatic radiation (laser beam). The laser light interacts with phonons or other excitations in the system, resulting in the energy of the laser photons being shifted up or down. The shift in energy gives information about the phonon modes in the system.

Light from the illuminated spot is collected with a lens and sent through a monochromator. Wavelengths close to the laser line, due to elastic Rayleigh scattering, are filtered out while the residual of the collected light is dispersed onto a detector. If the final vibrational state of the sample is more energetic than the initial state, then the emitted photon will be shifted to a lower frequency in order for the total energy of the system to remain balanced. This shift in frequency is designated as a *Stokes shift*.
If the final vibrational state is less energetic than the initial state, then the emitted

photon will be shifted to a higher frequency, and this is designated as an *Anti-Stokes shift*.

Usually with the term 'Raman spectrum' is considered the portion of the spectrum which contains the Stokes lines and it is a finger print of the sample.

The apparatus used in this thesis work is a micro-Raman spectrometer. It is composed of a multi-line horizontally-polarized c.w. Argon ions laser (maximum power: 100 mW, tunable in the 3 different lines of Ar^+ but utilized mainly with the fundamental one of 514.5 nm) , a triple-grating (300 - 600 - 1800 gr/mm) spectrometer (iHR550 - HORIBA JOBIN YVON) coupled with a liquid-nitrogen cooled multichannel charge-coupling device(CCD).
The spectrometer is ideal for a variety of research application, including: Raman spectroscopy (max resolution: 0.6 cm^{-1}) and photoluminescence spectroscopy . The microstage allows one to reduce the investigated area to less than 1 μm of diameter.

4.2.3 Reflection High Energy Electron diffraction (RHEED)

RHEED analysis has been performed by Prof. Marco Rossi, Dept. of Energetics, University of Rome 'Sapienza'. The set up (AFI EM6G) is equipped with a 60 kV working energy, high resolution diffractometer used in selected area configuration.
A goniometer enables the optimization the grazing incidence angle of the electron beam with respect to the sample and to move the sample itself parallel to the electron beam (i.e. to scan over the sample).

4.2.4 X-ray diffracion (XRD)

X-ray diffraction is a characterization technique regularly used to identify the different phases in a polycrystalline sample. Two of its most important advantages for analysis of materials are that it is fast and non-destructive.

When the positions and intensities of the diffraction pattern are taken into account the pattern is unique for a single substance. The X-ray pattern is like a fingerprint and mixtures of different crystallographic phases can be easily distinguished by comparison with reference data.

Usually electronic databases such as the Inorganic Crystal Structure Database (ICSD) are employed for this comparison. The major information one gets from this method is

the crystalline composition and the phase purity. Therefore the degree of crystallinity can be qualitatively estimated.

In particular XRD analysis has been performed in collaboration with Dr. Giorgio Cappuccio at the I.N.F.N.-L.N.F. institute (Frascati). The set up was constituted by a powder diffractometer (SEIFERT-XRD3003) with a Bragg–Brentano geometry, employing a Cu Kα source (λ= 1.54056 Angstrom).

4.2.5 Field Emission measurements (FE)

Electron emission from solids can be obtained via:

- photoemission
- thermionic emission
- field emission.

In the first two cases the electrons overcome the surface barrier by absorbing the needed energy in the form of photons or heat: A. Enstein [32] and O. W. Richardson [33], for photoemission and thermionic emission respectively, supplied the physical insights and mathematical descriptions of the phenomena which earned both of them the Nobel Prize.

But electrons emission can occur also by means of tunnelling through the potential barrier of the surface: the phenomenon is assisted by an intense electric field, so it is named field emission. The current generated through this process was fully described in the frame of Fowler-Nordheim theory [34].

In the experimental work described in this thesis, for some samples it has been possible to test their electronic properties by means of a home-made field emission apparatus (see a scheme in Fig. 4.2).

Roughly, field emission investigation requires the measurement of a current between two counterfacing electrodes (the anode, here called probe, and the cathode, i.e. the investigated sample) needing a good level vacuum and high voltage supply.

The FE measurement set up must satisfy two mandatory requirements:

1. vacuum requirement: pumps, valves, gauges, connections;
2. high voltage power supply and current measurement circuit.

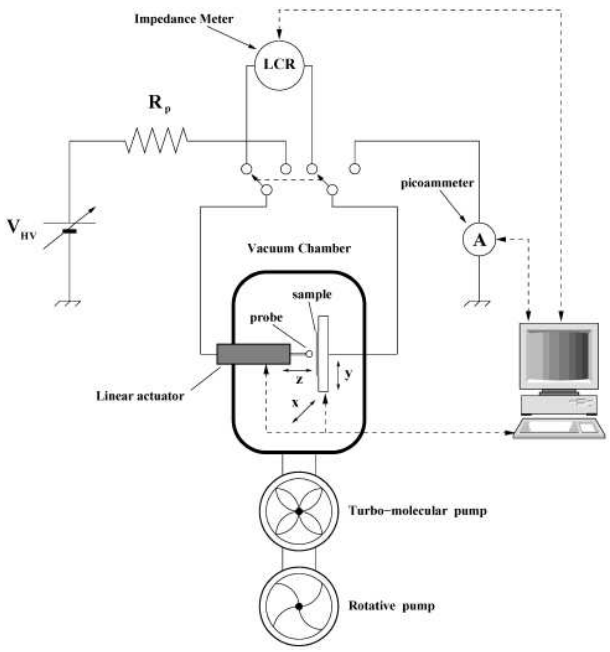

Figure 4.2: Scheme of field emission apparatus at the Dept. of Chemical Sciences and Technologies, University of Rome 'Tor Vergata.

Our set-up displays an optional requirement constituted by a probe (z direction) and sample (x, y directions) micro-movement system.

The core of our system is a stainless steel chamber with a number of flanges to allow evacuation of air, measurement of pressure, electrical contacts, anode-cathode movement system. The chamber is evacuated by a turbo-molecular pump with a rotative pump in series so that the lowest achievable pressure is of the order of 10^{-7} mbar.

The probe (anode) consists of a steel ball, with diameter of 2.0 mm; and it can move along the axis by means of a high resolution linear actuator, endowed with a theoretical 0.059 μm resolution. The actuator is provided with a DC motor driven by a PC via RS-232 through a controller whose minimum incremental step is 0.1 μm.

The power supply and measurement system is composed of a high voltage source, a picoammeter and a protection resistor. The high voltage source can deliver a maximum current of 3 mA when the maximum output voltage is limited to 3 kV (1 mA up to 8 kV).

The control of z motion and data acquisition is performed through a purpose realized software (LabVIEW). With our apparatus it is possible to make measurements both keeping constant voltage and varying anode-cathode distance and keeping distance fixed

and varying voltage. Current as a function of time can be recorded as well.

Finally, the effective anode-cathode distance is determined via the measurement of the anode-cathode capacitance using a LCR-meter (Stanford Research SR715 model).

4.3 Synthesis of CVD diamond from detonation nanodiamond: experimental conditions

P-doped Si(100) wafers cut in 1cm x 1 cm squared pieces have been used as substrates for all the syntheses shown in this section.

Diamond growth by means of CVD technique from detonation nanodiamond dispersion has been carried out following the well established experimental parameters usually used for the synthesis of polycrystalline diamond films in our labs.

A mixture of methane/hydrogen (1% CH_4 in H_2) is introduced in the reaction chamber and then, when the right value of pressure is reached, it is activated by the tantalum filament heated up to a temperature of 2200±10°C.
In a first stage, that is the nucleation step, the temperature of the substrate is maintained costant at 650°C for a time to allow the formation of *nuclei*. In the next stage the temperature of the substrate is raised up to 700°C and maintained throughout costant for the entire duration of the film growth.

As discussed in the previous section, it should be stressed that the key step in the CVD technology of this kind of growth is the creation of a high concentration of the *diamond nuclei*, by means of a *seeding* pre-growing step, onto the substrate and also the increase of the nucleation rate during the synthesis.

In this work of thesis, detonation nanodiamond as 'seeding material' has been used on the silicon substrate. in particular using different fractions of DND colloidal aqueous dispersion, a surface assisted self-assembly of the particles (with typical sizes in the range 4–10 nm) has been observed. As a consequence, different diamond *exotic architectures* have been produced.

4.3.1 Growth of *'shaped'* polycrystalline diamond films

A series of differently shaped free-standing nanodiamond structures has been prepared, analysed and used as templates for the growth of polycrystalline diamond layers by CVD technique.

The starting material for these experiments was detonation nanodiamond manufactured by the *Federal Research and Production Centre 'ALTAI'*(Russia), purified by oxidation and dispersed in aqueous medium.

A pale-grey colloidal suspension was obtained by moderate mixing of the native dispersion in a test-tube using sonication for 30 minutes. Slight colour changes along the tube length indicated the presence of compositional gradients.

The self-assembly of nanodispersed diamond into a solid structure is achieved by a solution phase method: the nanodiamond slurry, with pH of about 6, is deposited by means of drop casting onto the surface of the substrate and allowed to dry at room temperature.

A series of different substrates, such as glass plates, Si(100) and Si(111) wafers, has been employed in the present experiments. Controlled amounts of the suspension were drawn from three different zones of the test-tube, i.e. bottom, middle and top.
Different self-assembled micro-structures have been obtained using portions of the colloidal suspension taken from such different zones.

In particular, *'star-like'* structures have been produced using the suspension taken from the top, whereas cracked *'polyhedral-like'* forms were obtained from the bottom zone of the suspension, as depicted in Fig. 4.3 and Fig. 4.4. Samples obtained from the middle zone of suspension, not shown here, exhibited intermediate shapes.

The very poor adherence of the self-assembled nanodiamond to the various substrates made possible their easy manipulation without breaking: a weak mechanical shock allowed us to remove the shaped deposits of DND from the substrate. A series of these self-assembled structures was thereafter used as templates for diamond growth by our CVD technique.

Moreover by micromanipulation, slices of the star-like deposits or portions of the polyhedral deposits were transferred in the hot filament CVD reactor for the coating process. Some segments (see Fig. 4.5) were positioned in such a way that their end part was sticking out of the sample holder. A series of runs lasting 3 h was carried out using a mixture of 1% CH_4 in H_2.

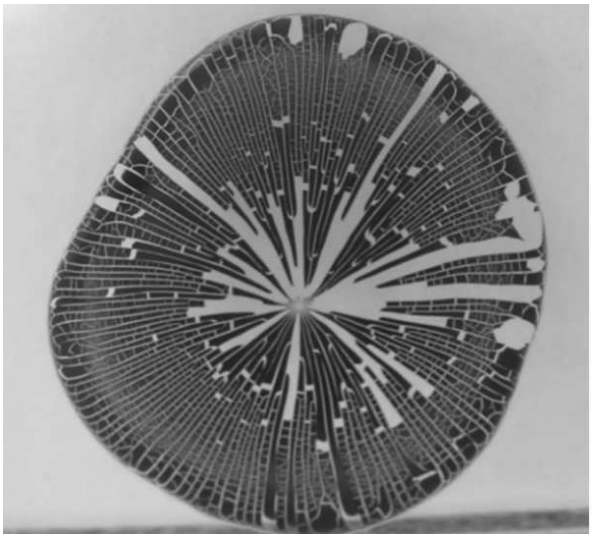

Figure 4.3: Optical image of the 'star-like' DND self assembled deposit.

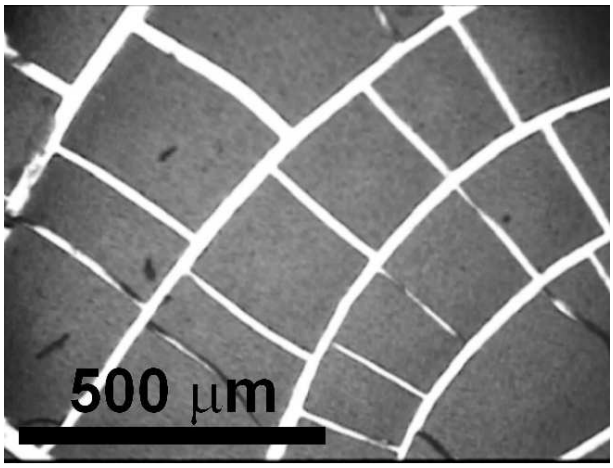

Figure 4.4: Optical image of the 'polyhedral-like' DND self-assembled deposit.

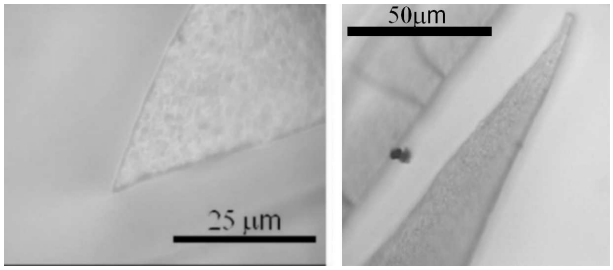

Figure 4.5: Optical images of self-assembled DND 'tips'.

It is to be noted that the features of these organized deposits are independent of the nature of the substrates and of their structure, i.e. amorphous or textured, and depend only on the fraction of the DND colloidal dispersion used.

The deposits reported in the present work have been generated under the following experimental conditions:

- Chamber pressure: 36 Torr
- Flow rate of the CH_4/H_2 mixture: 2/200 sccm (standard cubic centimetres per minute)
- Filament temperature: 2200±10°C
- Substrate temperature: 650°C during the nucleation stage and 700°C during the growth process.

After the coating process, all the samples have been characterized and the results obtained are discussed in the following section.

4.3.2 Morphological and structural characterizations: SEM, Raman spectroscopy, RHEED and XRD

Figure 4.6 shows FEG-SEM images of portions detached from typical deposits, transferred to the sample holder of the CVD reactor and submitted to the coating process. The diamond deposit preserved the architecture of the pristine DND templates.

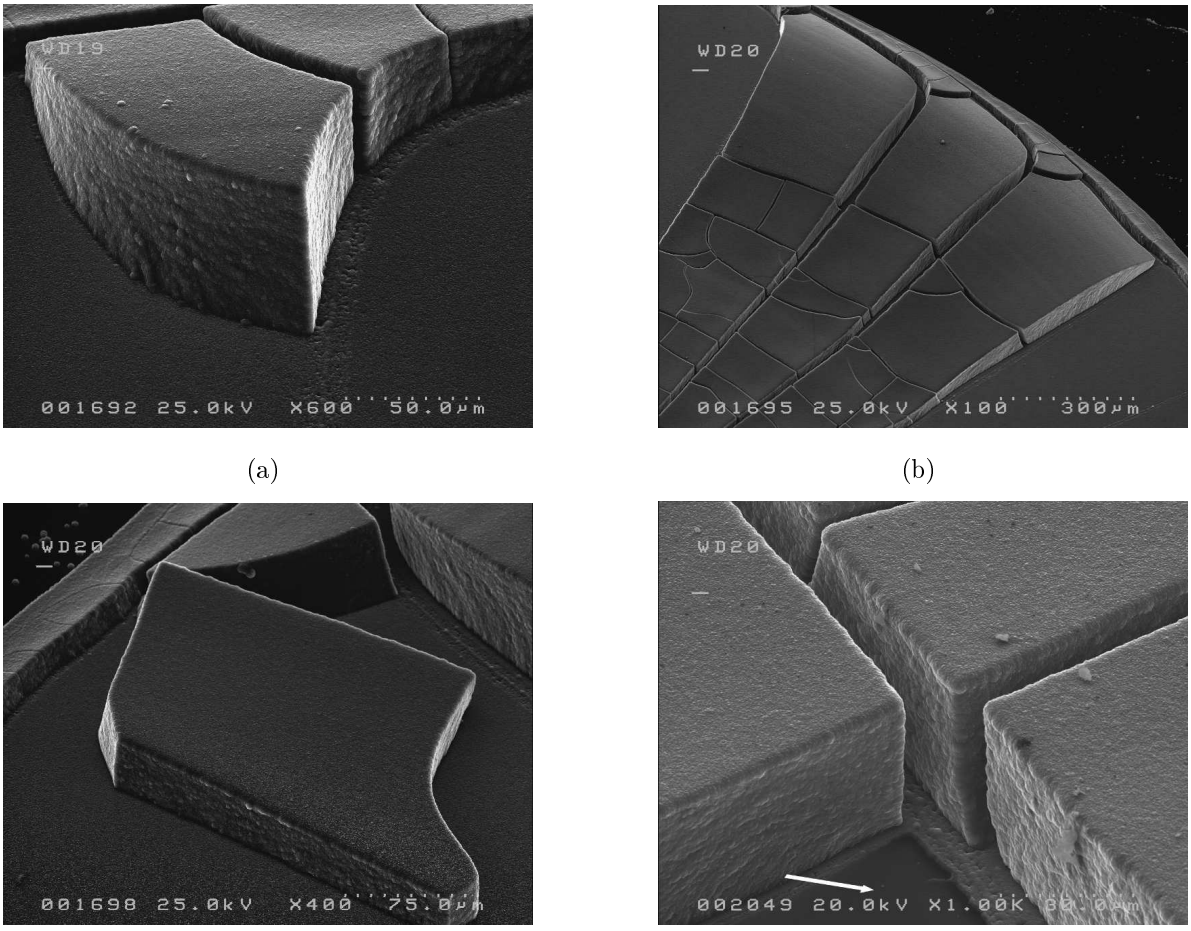

Figure 4.6: FEG-SEM images of CVD diamond films grown on self-assembled 3D nanodiamond structures:(a)-(d) monolithic deposits with polyhedral and rectangular shapes obtained from dispersion; the white arrow in (d) indicates the area from which a diamond microcomponent has been removed.

Moreover the preservation of the pristine geometry produces the formation of 'microchannels' among the polyhedral components of the deposit (as it can be see in Fig.

4.6(d)) which could be exploited as valid tool for the study of the emerging micro- and nanoscale transport phenomena which have applications ranging from unmanned aerial vehicles to ink jet printing to biochemical sensing, filtration and purification processes.

The next figures 4.7 show the typical 'tip' obtained from the star-like deposit and details of CVD grown diamond layers.

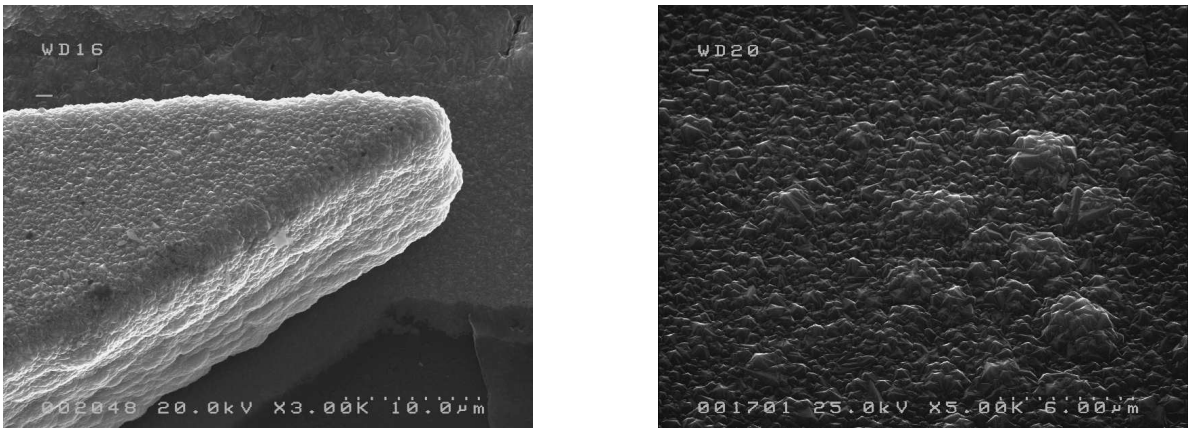

(a) (b)

Figure 4.7: FEG-SEM images of CVD diamond films grown onto the tip of a free-standing slice from a star-like deposit; (b) details of the polycrystalline layer coating the tip.

From the SEM images it has been possible to evaluate as the polycrystalline films deposited on the DND agglomerates were very uniform: the diamond deposition has been obtained on the edges of the cracks, on the faces between adjacent edges and also at the bottom side of the various segments.

By means of Raman spectroscopy, we have obtained information on the degree of phase purity of the CVD diamond coatings, as it can be observed in figure 4.8, where the two curves are related to the the sample before (a) and after CVD diamond film growth (b).

It has been found that there are not significance differences in the Raman spectra obtained for the two types of deposit, i.e. the star-like and the polyhedral one. For this reason the Raman spectra reported can be considered representative of both the shaped DND assemblies.

The results obtained confirm a high phase purity and match with the findings of the experiments performed using DND sprayed on various substrates as seeding for diamond

film growth [35, 36].

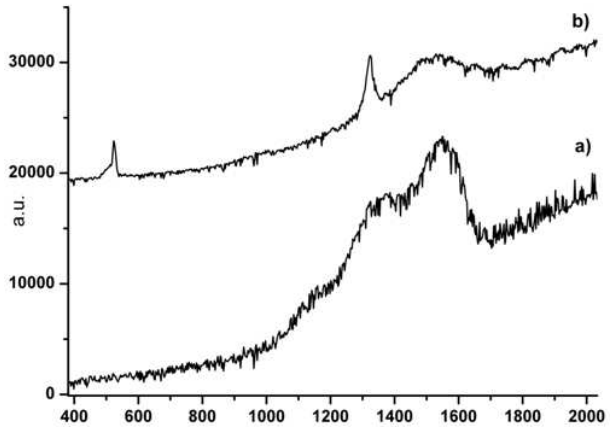

Figure 4.8: Raman spectra of DND structures (curve (a)) before CVD growth and of CVD diamond film (curve (b)) grown on DND self-assembled 3D structure.

The RHEED analysis of the coated deposits confirmed the presence of the diamond phase (space group Fd3m) for all the coated samples. In the case of the star-like coated samples, the presence of diffraction arcs in the experimental pattern (figure 4.9a) evidenced a textured structure with a preferential oriented growth towards the $\langle 110 \rangle$ direction, as can be deduced on the basis of the indexing reported in figure 4.9b.

Considering the relationship between real and reciprocal space, the length of the diffraction arcs (i.e. the corresponding subtended angle) can be used to achieve a quantitative indication about the degree of the preferred orientation.

For a cubic phase, subtended angles of $90°$ and $0°$ could be considered corresponding to a polycrystalline material without any preferential orientation and totally preferentially oriented, respectively.

The degree of orientation can be considered as the angular aperture of the cone in which a specific crystallographic direction is found for the different single crystallites forming the polycrystal. In the case of figure 4.9(b), that is the case of the star-like coatings, we determined a value of about $12.5° \pm 0.5°$ (corresponding to a solid angle of about 0.59 ± 0.05 srad) for $\langle 110 \rangle$ orientation.

Instead, the samples obtained from the polyhedral structures shown a lower orientation degree. These results suggested that the orientation features of the diamond layers deposited on the nanodiamond assemblies are strongly influenced by the structural organization of the underlying skeleton.

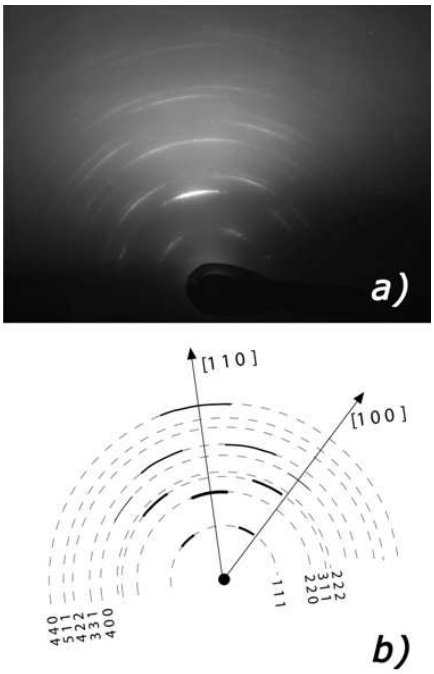

Figure 4.9: (a) RHEED pattern from a ⟨110⟩ oriented CVD diamond coating; (b) calculated pattern (dashed line) with indexing from the crystallographic data reported for the diamond phase in the ICDD-JCPDS database.

Finally, the x-ray diffraction spectra taken from the uncoated sample and from the same sample coated by CVD diamond, for the star-like assembly, are reported in figures 4.10(a) and 4.10(b), respectively. Both samples give rather broad diffraction signals at about 43.9° corresponding to the (111) reflection of diamond (JCPDS card: 6-675).

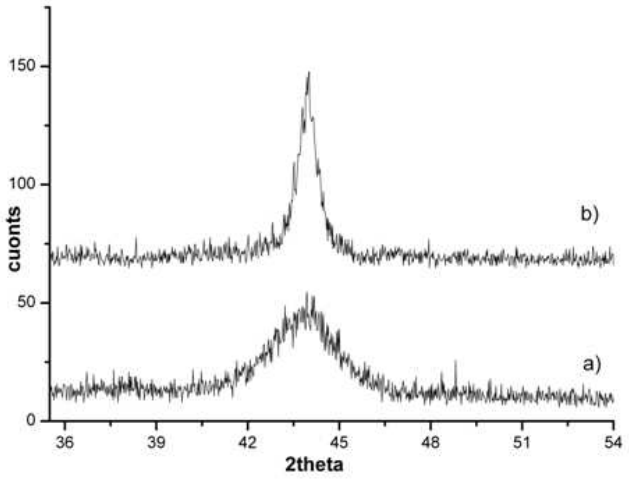

Figure 4.10: X-ray diffraction spectra from the star-like sample before (curve (a)) and after (curve (b)) CVD diamond coating.

Using the well-known Scherrer equation, from the full width half maximum (**FWHM**)of the (111) experimental reflection we estimated a crystalline size $\langle Lvol \rangle$ of 3.5 nm and of 22 nm, respectively, before and after the CVD diamond coating.

Some comments must be given on the differences in the self-assembly of the nanodiamond. This DND colloidal system was extensively studied by Larionova et al [37]: the agglomerate sizes, the dispersivity, the chemical properties and the electrokinetic potential of different fractions of the DND dispersions have been investigated using controlled centrifugation and the FTIR technique.

The data [37] evidenced the presence of three principal fractions: a first one with larger aggregates and white–grey colour, a second fraction with medium size aggregates and brown–black colour, and a third with smallest aggregates and black colour.

These fractions were found to differ each from the other not only in particle size but also in the surface chemical properties. In this contest it is not surprising that fractions with agglomerates characterized by different sizes and moreover different surface chemistry tend to assemble in different forms, such as fibres, whiskers and dodecahedral quasicrystals [38, 39].

The literature results strongly suggest that the driving force for the self-assembly of nanodispersed diamond in a liquid phase is a supramolecular mechanism induced by the dipole moment of the nanosized aggregates. In the case of the formation of DND structures onto a substrate, as in the present experiments, it must be considered also a surface assisted mechanism, according to the results reported in [40, 41], that helps in promoting the cooperative interaction between DND building blocks.

4.4 Synthesis of diamond films on patterned NbN/Si substrate: experimental conditions

The NbN substrate were realized at the Dept. of Physics, University of Rome Tor Vergata. The NbN layers have been deposited by DC-RF Magnetron sputtering by means of controlled experimental parameters on silicon commercial wafers. The NbN film are 400 nm thick. In order to compare the diamond growth process on NbN and Si surface, we have produced patterned substrate by masking a selected area of Si substrate during the NbN deposition. With the aim to study the kinetic of the CVD diamond growth on the NbN substrate and to evaluate the ideal experimental conditions to obtain polycrystalline films with good morphological and structural properties, we have performed 4 runs of CVD diamond synthesis by using the experimental parameters listed in the following:

- filament temperature: 2100±10°C;.
- substrate temperature: 650°C±10°C;
- typical filament/substrate distance: 10mm;
- H_2 flow: 198 sccm;
- CH_4 flow: 2 sccm;
- synthesis time: 10 minutes, 30 minutes, 1 hour and 3 hours.
- No seeding pretreatment onto any sample.

We preferred to fix the synthesis conditions and vary the time of growth rather than the opposite because temperature, distance between filament and substrate have already proved successful for all previous synthesis experiments.

4.4.1 Morphological and structural characterizations: preliminary results

By the SEM analysis of the samples grown with different synthesis times, we could investigate the growth evolution of the nanocrystalline diamond frame-to-frame. For every sample we reported the morphology both of the NbN coated Si part and of the bare Si one in order to estimate if there were differences in the diamond growth onto the two parts of substrate.

From Fig. 4.11 the morphology of the deposit grown for 10 minutes on the NbN surface can be observed. The information gathered from this analysis, at very beginning, highlights a number of interesting features.

For comparison we reported in the following the SEM analysis of the diamond deposit synthesised on bare Si substrate (see Fig. 4.12).

As it can be observed, in the case of diamond deposited on the NbN surface, the SEM images showed a large area coated by diamond nanocrystals, most of them tending to coalesce to form nanodiamond chains. Moreover a good crystallographic quality is evidenced in the higher magnifications images in which, although there were some difficulties because of the the strong insulator behaviour of the crystals, we can recognize pronounced edges (see Fig. 4.13).

In Fig. 4.12 , it can be observed as also the Si surface appeared coated by diamond nanocrystals but the scarcity of the deposit, let us to suppose that the absence of the NbN layer lead to a slower nucleation rate and growth. In fact, from the Fig. 4.11(b) and Fig. 4.12(b), we have estimated the average density of nuclei which covered an area of about 100 μm^2 on both the substrate, obtaining a value of 0.3 nuclei/μm^2 and 0.6 nuclei/μm^2 for Si and NbN surface respectively.

After 1 hour of CVD deposition, the morphology and crystallographic habit of the diamond crystals appeared more defined and also an estimation of the average dimensions could be obtained, as depicted from the detail of in Fig. 4.14.

The results obtained after 3 hours of diamond deposition on NbN surface and Si are finally showed in Fig. 4.15 respectively.

As it can be noticed, for longer time of synthesis we do not obtain a homogeneous and continuous film but the influence of NbN layer for the rate of diamond growth is strongly evident, clearly depicted from the density and quality of the diamond deposits produced.

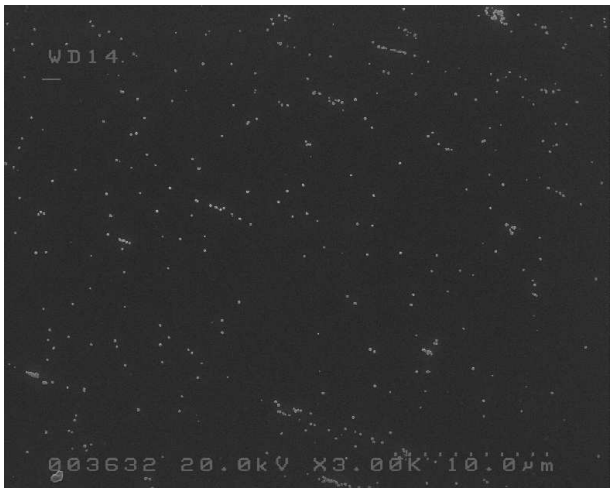

(a)

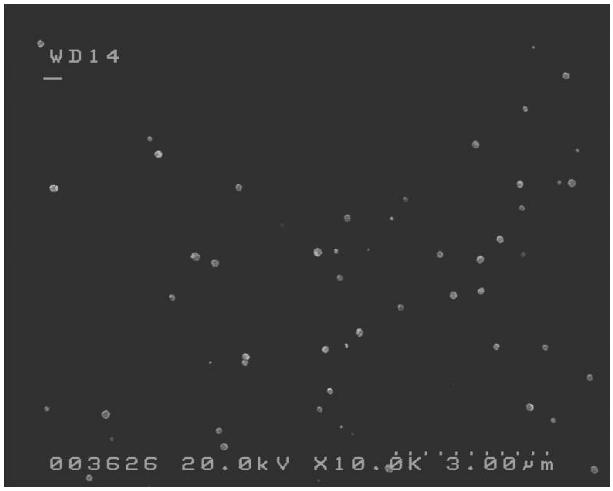

(b)

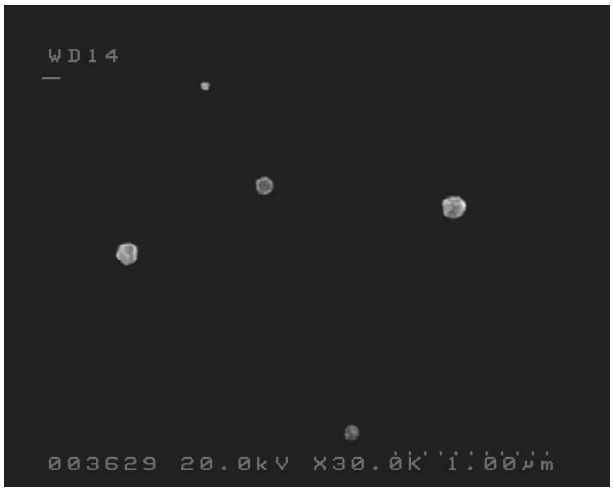

(c)

Figure 4.11: (a) FEG-SEM images of early stage of the diamond growth (after 10 min.) onto the NbN surface; (b)-(c) higher magnifications with details of the deposit.

(a)

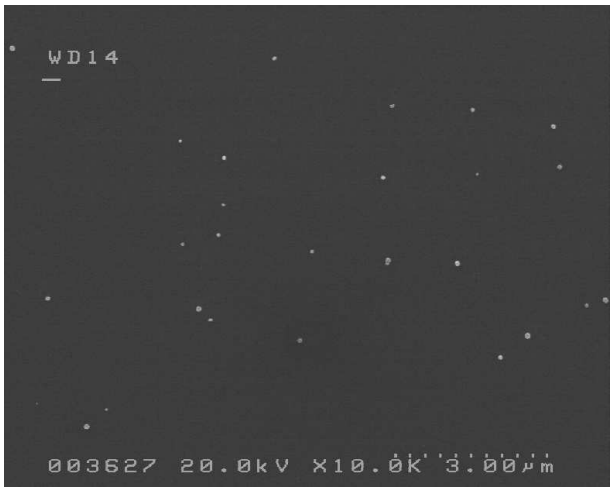

(b)

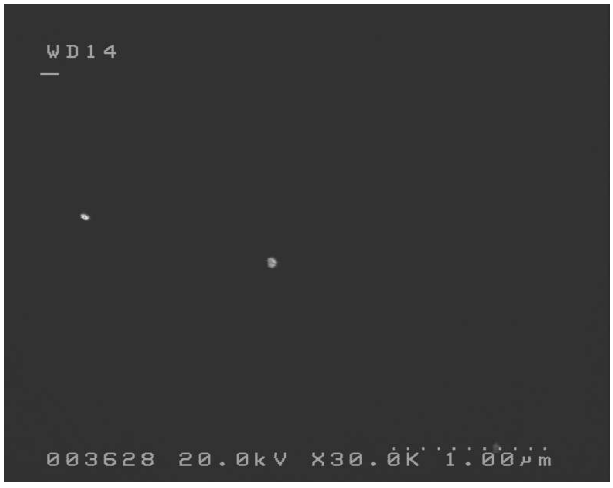

(c)

Figure 4.12: (a) FEG-SEM images of early stage of the diamond growth (after 10 min.) onto the silicon substrate; (b)-(c) higher magnifications with details of the deposit.

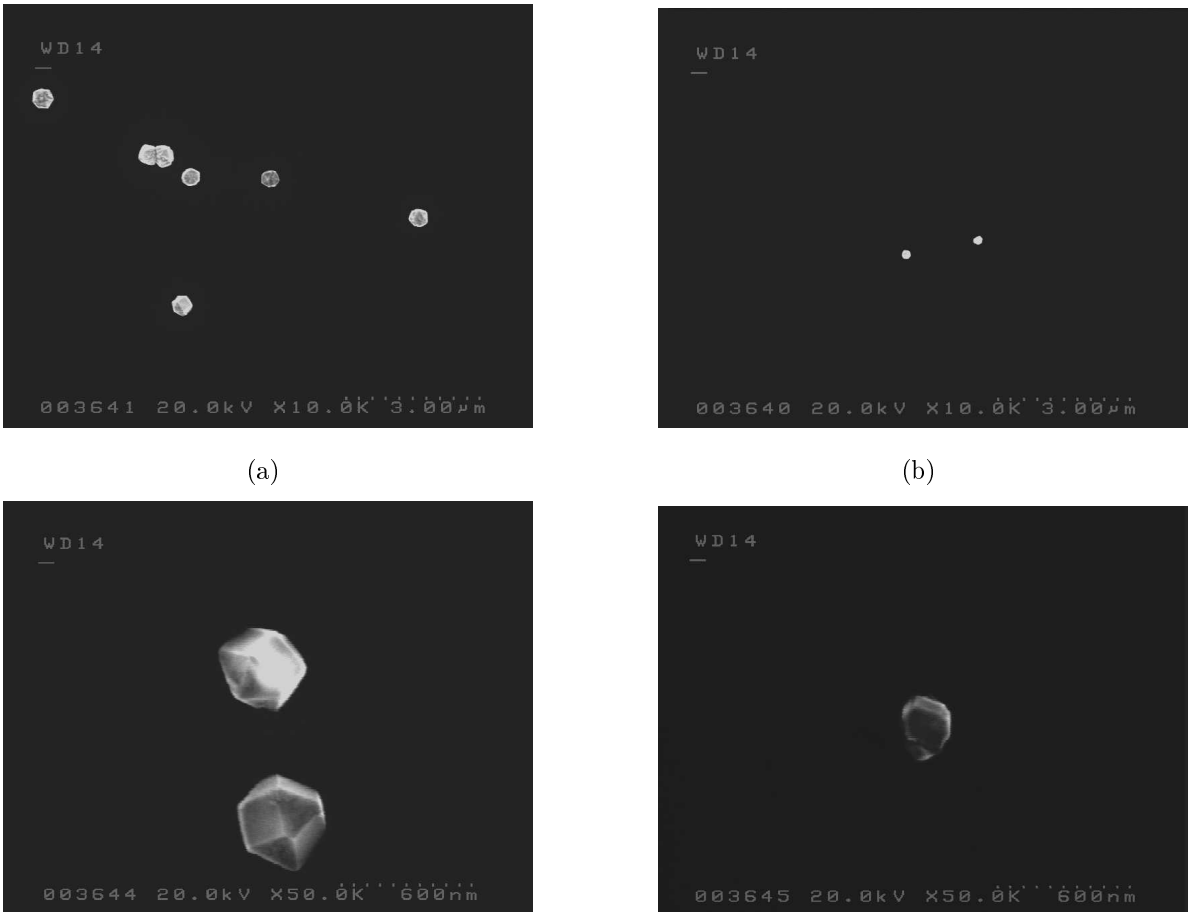

Figure 4.13: FEG-SEM images of the diamond growth after 30 min.: (a)-(c) onto the NbN and (b)-(d) on Si substrate.

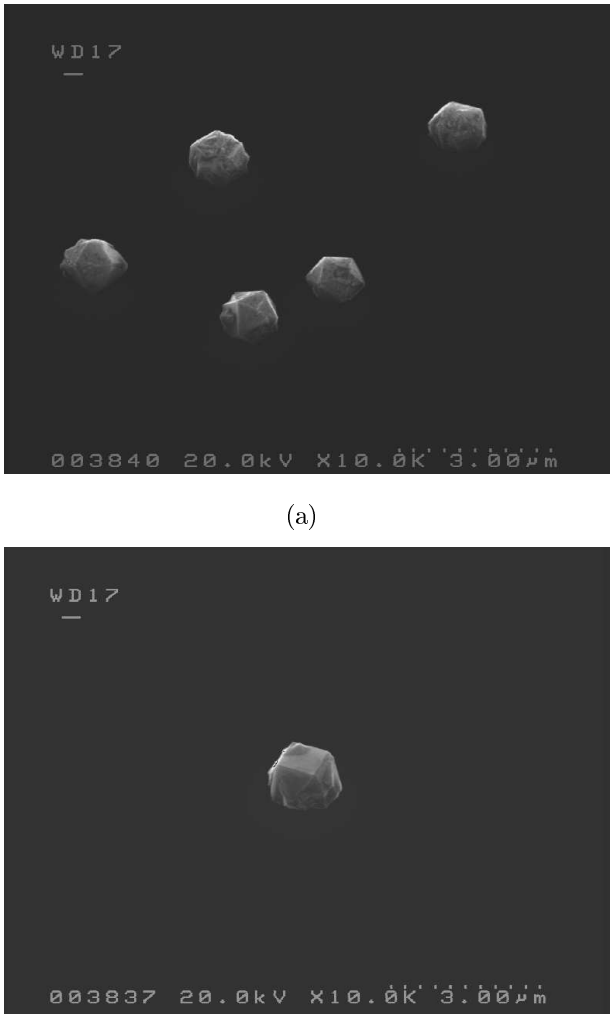

(a)

(b)

Figure 4.14: FE-SEM images of the diamond growth after 1 hours: details from (a) the NbN substrate; (b) bare Si.

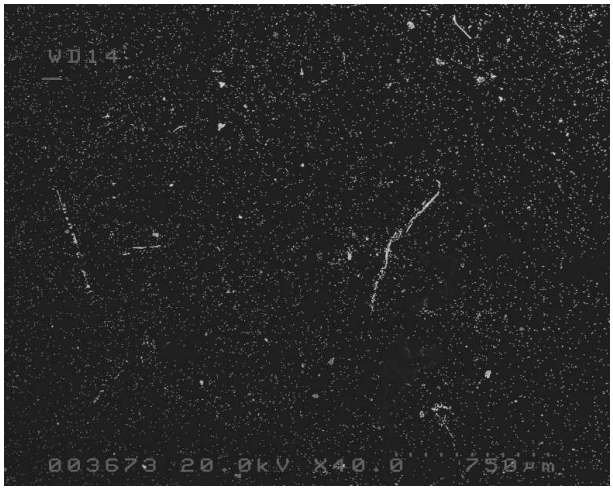

(a)

(b)

Figure 4.15: FEG-SEM images of the diamond growth after 3 hours: (a)onto the NbN coated Si substrate; (b) on bare Si.

Summarizing, from short time of synthesis (10 minutes) we have evaluated the density of the diamond nuclei produced onto the two different substrates (NbN and Si) without any seeding process on them. The higher density of diamond crystals present on the NbN coated substrate than on the bare silicon one suggests that diamond has NbN as preferential substrate. This is traduced in a higher number of 'nuclei' produced on NbN.

At the same, with longer time of deposition (from 30 minutes to 3 hours at least) we were able to evidence the sizes and shape of the diamond crystals, which ranged from few hundreds of nm to about 1 micron.

An important experimental aspect that we could observe is related to the resistance of NbN layer to the bad effect of hydrogen plasma etching exploited from the surface during the entire synthesis process. The behaviour of NbN in drastic conditions plays a fundamental role in the view to produce material for electronic applications.

To exploit and confirm the survival of the NbN layer onto the silicon substrate after diamond growth, XRD measurements and Raman spectra have been collected for all the samples produced. In the following (Fig. 4.16) we reported a Raman spectrum which can be considered representative of all the sample obtained. It clearly shows the indexed Raman peak of diamond centred at 1337 cm^{-1} (vs the value of 1332 cm^{-1} from the literature), while the presence of NbN cannot be detected with this technique and for this reason we have performed x-ray analysis.

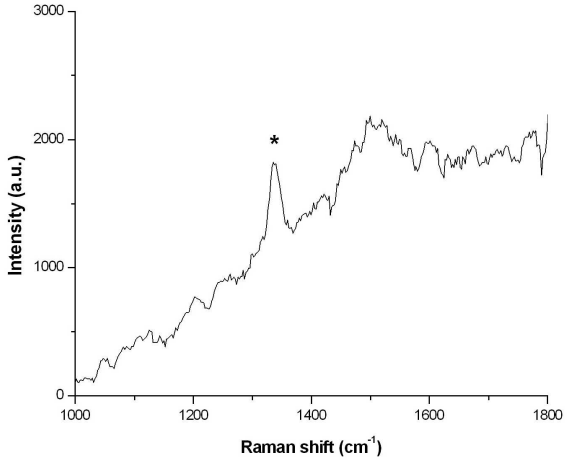

Figure 4.16: Raman spectrum of diamond deposit on the NbN substrate.

In the following we show the results obtained from XRD analysis in terms of evolution of the NbN layer during the 4 synthesis runs (see Fig. 4.17).

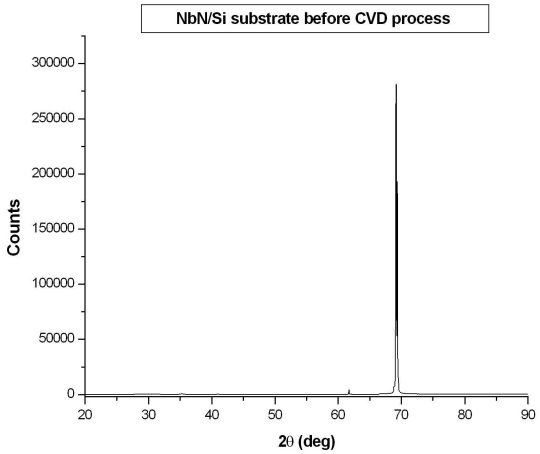

(a)

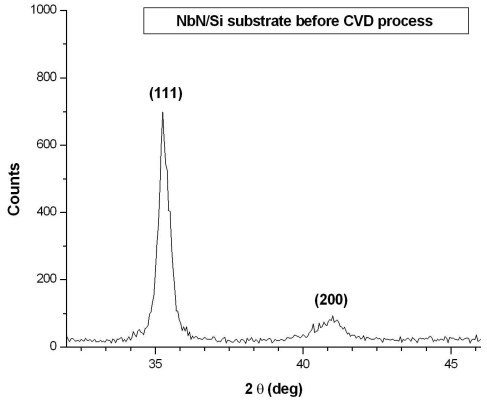

(b)

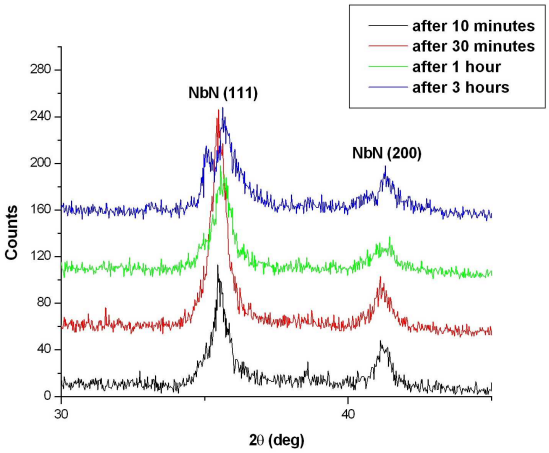

(c)

Figure 4.17: XRD spectrum of: (a) NbN/Si substrate before CVD growth; (b) inset with NbN reflections; (c) NbN/Si substrate after the synthesis runs.

First of all, as it can be observed from Fig. 4.17(a), we have collected the XRD spectrum for the pristine NbN coated Si substrate in order to evaluate the presence of the NbN layer and to study the crystallographic features of the coating.

As it can be observed, the strong signal centred at 2theta value around 69° is the well known reflection (400) of the perfect crystalline Si substrate (JCPDS card: 27-1402) but it covered the reflections attributable to NbN layer.
For this main reason we have performed the other XRD measurements by using a 'theta scan' (or a quasi-grazing incidence diffraction - GID) which consisted of fixing theta at the value of 5° (vs the substrate) and scanning the 2theta values in a predefinite range.

In particular all the spectra related to the samples prepared in the 4 synthesis runs have been collected in the range from 30° to 45° because the two main reflections for cubic NbN (JCPDS: 38-1155) are centred at the 2 theta values of 35.36° for (111) and 41.07 for (200) respectively.

The figure 4.17(c) showed the data obtained under the experimental conditions reported above and from the comparison of all the spectra registered we can confirm that the drastic conditions generated during the CVD growth (caused by high T and the strong concentration of hydrogen) didn't modify substantially the characteristics of the NbN layer which seems to remain unaltered.

4.5 Synthesis of diamond films on multifinger $Si/SiO_2/NbN$ device

Starting from the previous results, we have carried out CVD diamond synthesis onto a patterned substrate constituted of a $Si/SiO_2/NbN$ interdigitated electrodes of a multifinger device. The experimental parameters adopted were the ones optimized in the previous experiments and are listed below:

- filament temperature: 2100°C±10°C;
- substrate temperature: 700°C±10°C;
- working pressure: 36 Torr;
- CH_4 flow: 2 sccm;
- H_2 flow: 200 sccm;
- synthesis time: 1 hour
- pretreatment of substrate by means of acetone solution of micrometric diamond powders.

In the following the FEG-SEM analysis is reported, Fig. 4.18.

The SEM analysis revealed that after 1 hour of synthesis, we obtained a 'quasi-continuous' polycrystalline diamond film which highlighted the catalytic effect of NbN layer. Particularly interesting is the fact that diamond preferentially grows on the NbN template than the bare SiO_2 leading therefore to the production of a *patterned deposit*. This selective diamond deposition could have useful implications in the integration of diamond in advanced devices.
The good quality of the crystals obtained are evidenced in Fig. 4.18(b) whereas the Raman analysis did not reveal any particular difference in the diamond structure of different areas of the sample.

As representative of all the collected data, Fig. 4.19 shows the Raman spectrum of the deposit.

As indexed in the figure, the sharp peak centred at 1339 cm^{-1} is attributed to the well known peak of diamond (from literature 1332 cm^{-1}) while the broad band around

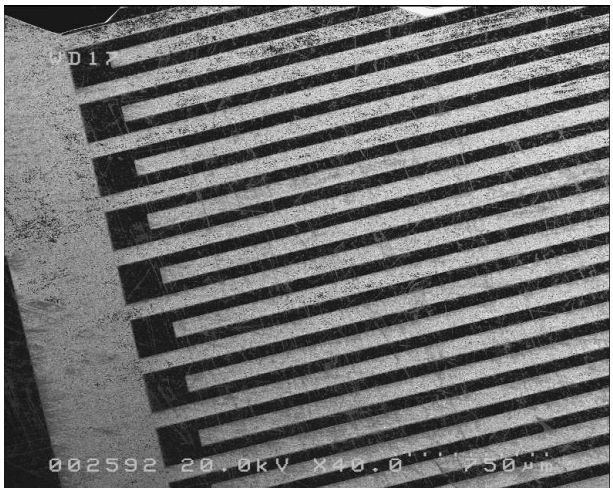

(a)

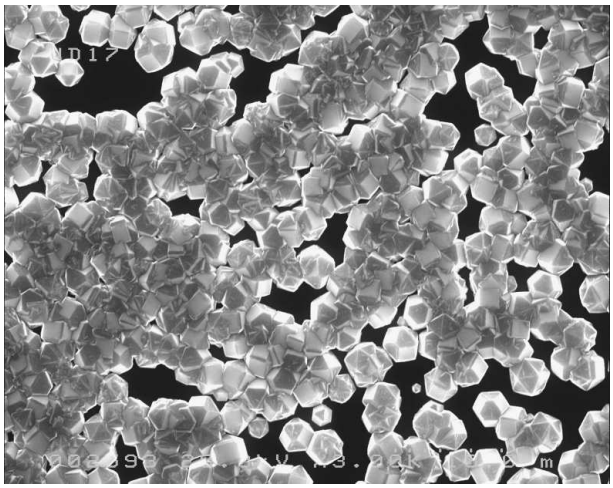

(b)

Figure 4.18: FEG-SEM images of the diamond growth after on a $Si/SiO_2/NbN$ multi-finger device: (a) general view; (b) details of the deposit.

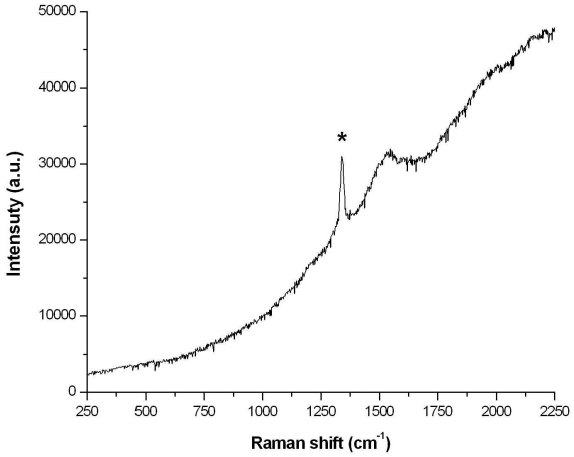

Figure 4.19: Raman spectrum of diamond deposit on the multifinger $Si/SiO_2/NbN$ device

1600 cm^{-1} and the luminescence one are generally attributed to the defects (in form of Csp^2) present in the diamond deposit.

The Raman spectroscopy was also widely used to study and analyse the residual stress within the CVD films. Strictly the Raman line shape is sensitive to the environment of the probed atoms and therefore indicative of local strain.

In the elastic regime, the strain of a free-standing crystal can be related to the applied stress by certain elastic compliance constants. In particular a Raman line shifts to higher and lower frequency under compressive and tensile stresses respectively.
The residual stress results from the sum of thermal strains, epitaxial strains, and the growth strains [42].

In our case the epitaxial strains are negligible. The thermal strain ($\sigma_{thermal}$) derive from the different thermal expansion coefficient of diamond and substrate and can be calculated by means of a general equation from [43] reported in the following:

$$\sigma_{thermal} = \frac{E}{1-\nu} \int (\alpha_f - \alpha_s) dT \tag{4.1}$$

(integrating between 20°C and the growth temperature T).

In this equation E is the Young's modulus, 1050 GPa (for polycrystalline CVD diamond), α_f and α_s are the thermal expansion coefficients of the film and the substrate respectively, ν is the Poisson ratio of the film (0.07 for CVD polycrystalline diamond) and T the growth temperature (in our case equal to 700°C).

Another source of stress could be due to the growth strain, i.e. a density charge during the film growth. For diamond grown by CVD, common growth strains may include graphite inclusions, hydrogen clusters and voids. The stress induced by growth strain is often called *'intrinsic'* stress [44, 45].

Using the shift of the position of Raman diamond peak is possible to calculate the magnitude of residual stress in CVD diamond films. In particular for polycristalline CVD diamond films the equation from [43] is:

$$\tau = -1.08 GPa/cm^{-1}(\nu_{exp} - \nu_{teo}) \tag{4.2}$$

By applying Lorentzian fitting for the deconvolution of the diamond Raman peak from spectra collected in ten different points of the sample both on the NbN layer and on the silicon oxide, we obtained average value of 1341.06±0.78cm^{-1} for diamond onto NbN substrate and 1339.37±0.64cm^{-1} for diamond on silicon oxide.

By using the equation 4.1 and equation 4.2 reported above and the reference data for CVD polycrystalline diamond and silicon oxide, we obtained the results showed in the following table:

	Total stress (τ)	Thermal stress ($\tau_{thermal}$)	Growth stress (τ_{growth})
NbN substrate	-9.8 GPa	**-7.1 GPa**	-2.7 GPa
SiO_2 substrate	-8.0 GPa	**-0.3 GPa**	-7.7 GPa

Figure 4.20: Stress value obtained for the CVD diamond polycristalline films on NbN and SiO_2

Note that for polycrystalline CVD diamond we used α_f of $0.8 \cdot 10^{-6}$K^{-1}, while for α_s value we used $10 \cdot 10^{-6}$K^{-1} for NbN layer and $0.5 \cdot 10^{-6}$K^{-1} for silicon oxide respectively.

As can be evaluate from the values reported in the table, the total stress estimated for the polycrystalline diamond grown both on NbN and on SiO_2 do not show a significant difference. At the same time it could be noticed that the thermal component has a large influence in the case of diamond grown onto the NbN layer and this result reflects the discrepancy in the value of thermal expansion coefficient between the two substrates used.

In the case of diamond grown on silicon oxide we can observed the opposite behaviour, as expected from its value of thermal expansion coefficient. Concluding, probably the diamond grown on the NbN substrate is more affected from thermal stresses although more stable mechanically, if compared to its analogous grown on SiO_2.

4.6 Synthesis of hybrid Csp^2-Csp^3 materials: synthesis strategy and experimental results

As described in the chapter 2 by the use of C nanopowders or methane as percursors within the right value of pressure, temperature and catalyst, SWCNTs or MWCNTs can be produced with our HFCVD apparatus. Moreover thanks to the versatility of our set-up, in a previous work [4], an one step synthesis approach has been carried out as a valid experimental route to produce ordered arrays of rigid nanotubes coated by diamond nanocrystallites.

In this section, alternative experimental routes with the same purpose of producing hybrid systems constituted by covalent bonded nanocrystalline diamond onto CNTs are presented. In particular the strategies investigated, provided the study and the application of experimental parameters usually adopted for the CVD growth of CNTs and diamond in a sort of *'mixed way'*. It means that:

1. in the first experiment the synthesis typical conditions for diamond growth (i.e CH_4 at 1% diluted in H_2) are used in presence, at the same time, of metal catalyst and high substrate temperature (T=900°C);

2. in the second the CNTs growth parameters (i.e. CH_4/H_2 flow rate of 10/100sccm) are adopted in absence of the catalyst and with low substrate temperature (T=700°C, t=3 hours);

3. a third alternative preparation route of hybrid CNT/nanodiamond structures is explored: it consists of using as template for the CVD diamond growth, SWCNTs grown by HFCVD (from C nanopowders) and case commercial SWCNTs (this last material could be suitable to be scaled up and adapted to the requirements of electronic industries) respectively.

After the syntheses, the samples have been characterized by means of electron mycroscopy, Raman spectroscopy, electron diffraction (RHEED) for what concerns the structural and morphological aspects while by means of our field emission apparatus a functional characterizations has also been performed.

By the SEM analysis of the samples grown with different synthesis times under the first condition listed above, we investigated the growth evolution of the nanostructures frame-to-frame and the ratio between the two components of Csp^2 and Csp^3.

In Fig. 4.22 we can see as from the very beginning *'sheet-like'* nanostructures appeared until after 30 minutes of growth a dense deposit of randomly distributed nanostructures can be evidenced.

The Raman spectrum is reported in Fig. 4.21.

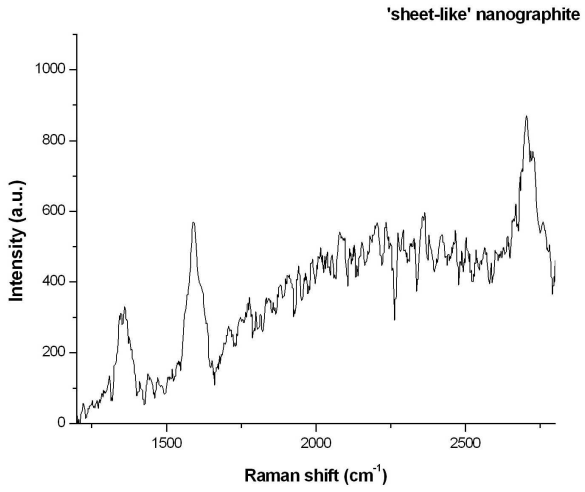

Figure 4.21: Raman spectrum of 'sheet-like' graphite deposit.

From the spectrum analysis it has been possible to obtain some information related to the chemical species present on the samples in terms of hybridization state of carbon. The Raman signals present in the spectrum are usually attributed to nanosized graphite and in particular:

1. the two peaks in the range between 1200 and 1600 cm^{-1} are usually assigned to D (it is related to the presence of defects) and G (crystalline graphite) bands respectively for graphite based materials with nanometric dimensions [46, 47];

2. the peak around 2700 cm^{-1} is attributed to the second order signal of the G band.

In the second type of experiment again a single step growth of CNT/nanodiamond hybrid was performed and from the SEM analysis, the presence of 'ball-like' deposit has been observed (Fig. 4.23).

In some points it can be seen as the structures tend to coalesce and for high magnifications, the presence of nanometric material on the surface of the 'ball' can be evidenced. This is usually related usually to a diamond synthesis growth in excess of carbon versus hydrogen.

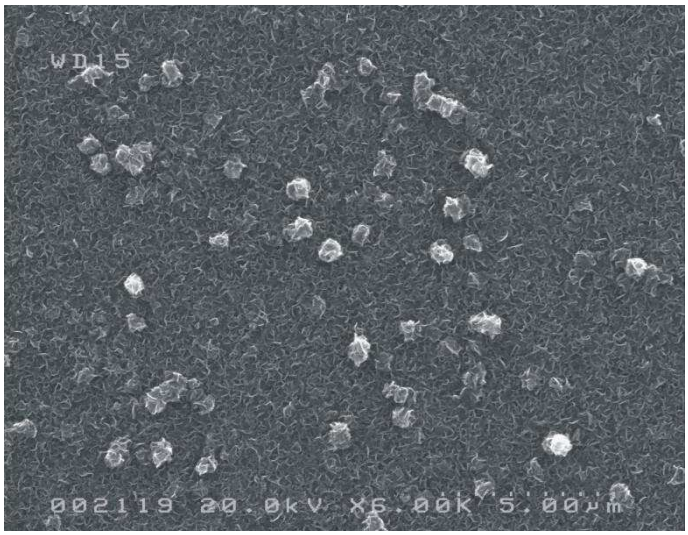

(a)

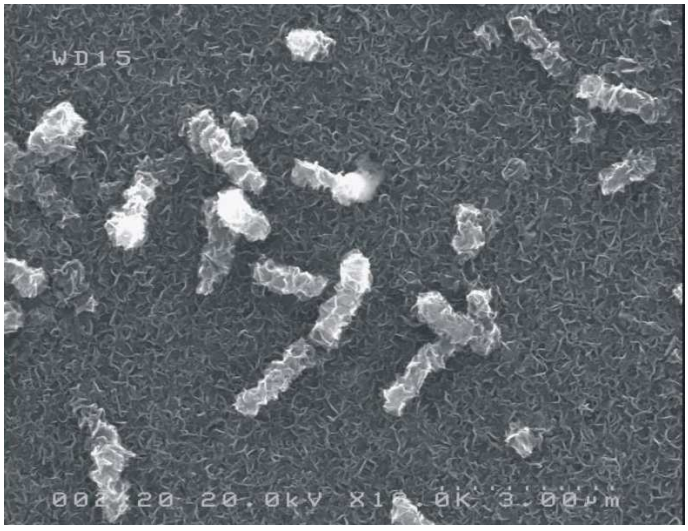

(b)

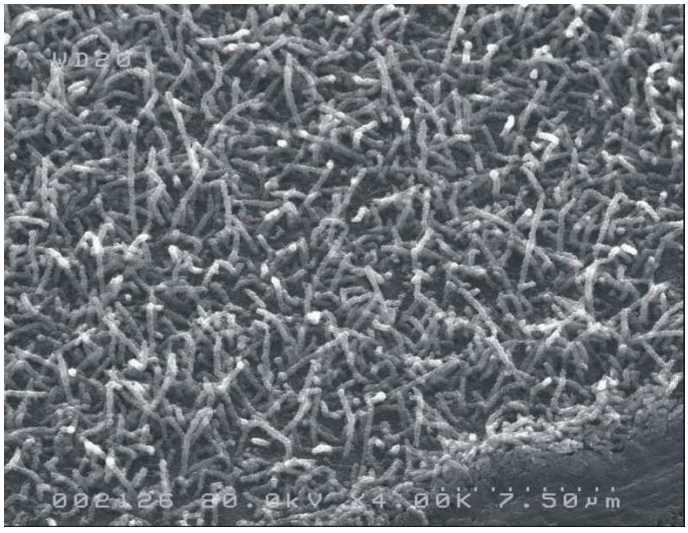

(c)

Figure 4.22: SEM images of the 'sheet-like' graphite after: (a) 5 min., (b) 15 min., (c) 30 min. of growth.

(a)

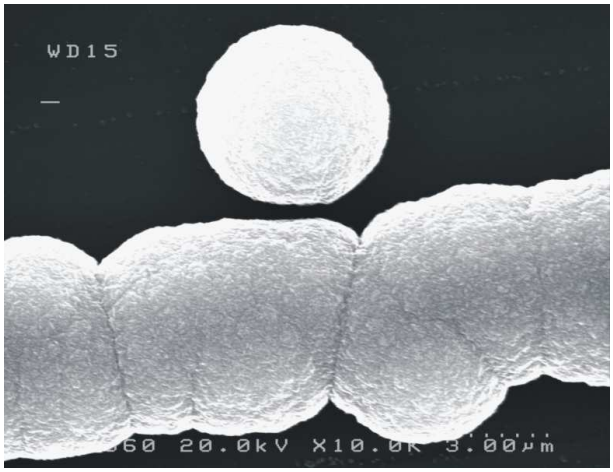

(b)

(c)

Figure 4.23: SEM images of the 'ball-like' deposit: (a) general view, (b)-(c) details of the deposit.

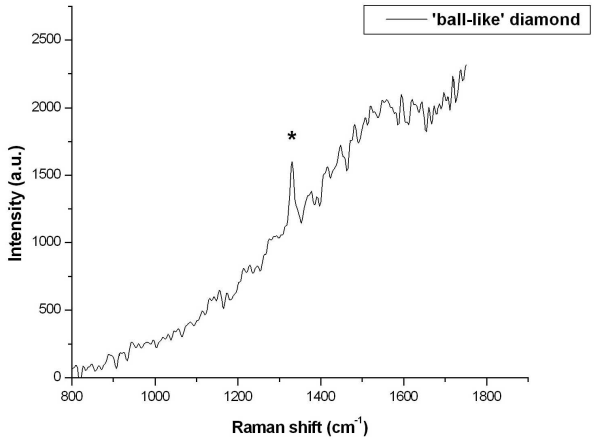

Figure 4.24: Raman spectrum of diamond 'ball-like' deposit

From the Raman analysis (see Fig. 4.24) we can estimate the presence both of the Csp^2 and Csp^3 amount since all the collected data showed the diamond peak (centred at 1332 cm^{-1}) and the graphite peak (centred at 1582 cm^{-1}). Moreover the presence of a broad signal in the range of the graphite peak gives information about the presence of sp^2 hybridized carbon.

In concluding, from the preliminary results obtained with these two synthesis approaches we found that by using the synthesis conditions for the diamond growth but in presence of the metal catalyst and high substrate temperature, the deposit obtained was constituted mainly of Csp^2 structures with a high defect degree (as confirmed by Raman spectrum also) and with 'sheet-like' structures. On the other hand by using the typical CNTs growth conditions in absence of metal catalyst and with a low substrate temperature, a diamond ball-like deposit was produced, confirming that none of the two previous steps exploited are able to produce CNT/nanodiamond hybrids.

As consequence of these results the CNTs has been used as template for the CVD diamond growth. In SEM images of Fig. 4.25 we can observe as the diamond growth proceeds onto a SWCNTs deposit (previously synthesised) from 30 minutes to 3 hours.

At least after a 3 hours deposition a more dense deposit constituted by larger diamond nanocrystals attached to some CNTs bundles has been evidenced (see Fig. 4.26). However because of the inhomogeneity of the sample,a significative Raman analysis cannot be performed.

The information gathered from the SEM analysis highlights a number of interesting

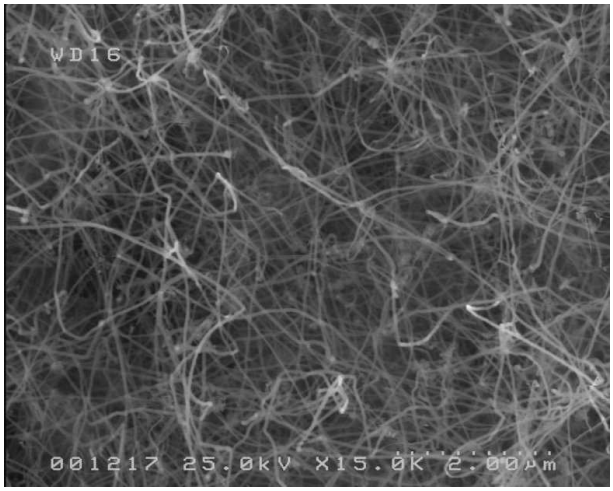

(a)

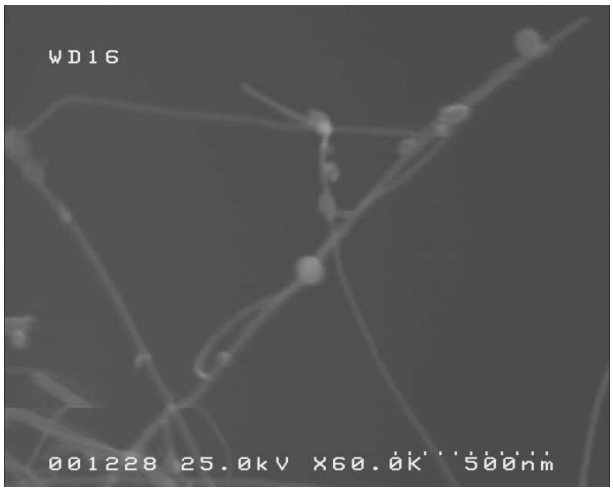

(b)

Figure 4.25: FEG-SEM image of diamond nanocrystals grown on SWCNT bundles:(a) pristine deposit; (b) after 30 minutes.

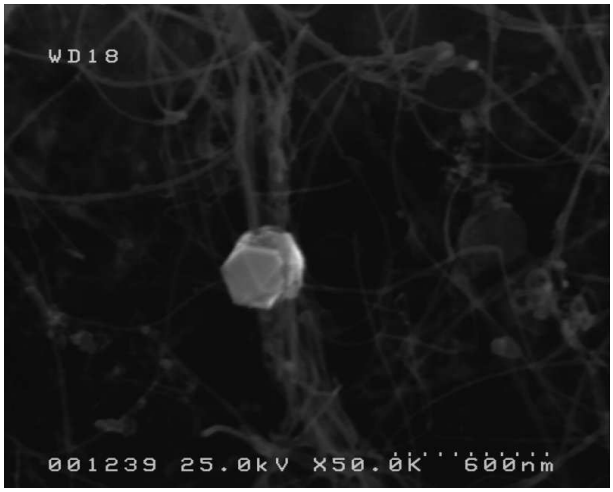

(a)

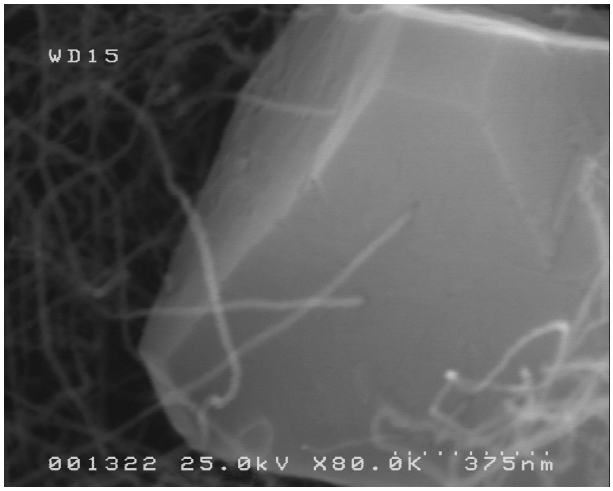

(b)

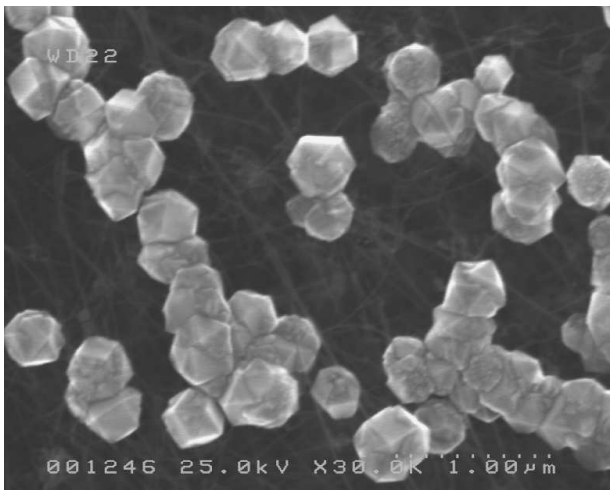

(c)

Figure 4.26: FEG-SEM image of diamond nanocrystals grown on SWCNT bundles:(a) after 1 hour; (b)-(c) after 3 hours.

features. For example, it is clear the presence of the hybrid system constituted by the CNTs and nanocrystalline diamonds. First of all it can be noticed as:

- the experimental conditions adopted lead to a high growth rate producing a deposit characterized by thin SWCNTs bundles, from the Fig. 4.25(a);
- the presence of the crystals with nanometric dimensions located most of all on surface of some CNTs bundles (Fig. 4.25(b));
- finally, in Fig. 4.26(a), it can be observed a large area of CNTs deposit coated by diamond crystals with well shaped facets and with dimensions under 500 nm.

In alternative, the coating by CVD of commercial single wall carbon nanotubes with crystalline diamond nanoparticles was performed. In this experimental route, SWCNTs from Cheap Tubes Inc. (diameters in the range 1–2 nm, lengths in the range of 10–30 μm) have been used. The nanotube layers were deposited on Si(100) plates by drop casting of dispersions prepared adding 2 mg of the purified material to 25 ml of methanol.

The coating of the SWCNT deposits by diamond was carried out in our HFCVD reactor, where the gaseous phase is activated by the Ta wire kept at 2200±10°C. The reactant used was a mixture of 1% CH_4 diluted in H_2. The main parameters for the synthesis runs were:

- gas flow: 200 sccm
- substrate temperature: 630±5°C
- working pressure: 36 Torr
- the runs lasted from 5 up to 30 minutes.

Characterization of these samples before and after the coating process has been carried out by FEG-SEM, by Raman spectroscopy and by RHEED.

The FEG-SEM image of a representative sample obtained by a 30 min lasting CVD run is shown in Fig. 4.27. The SWCNT bundles, entangled, and randomly positioned along the Si (100) substrate, appear uniformly coated by a nanocrystalline deposit.

The RHEED pattern, the indexing and interplanar spacings obtained (Fig. 4.28) are in a nearly ideal agreement with the reference data for Fd3m diamond phase (ICCD Database PDF:06–0675; CDF:037638).

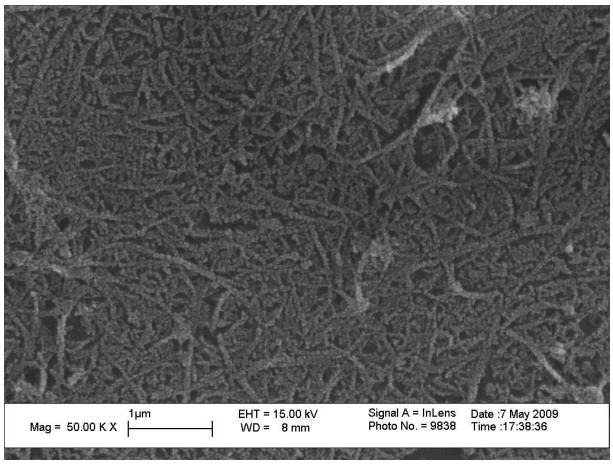

(a)

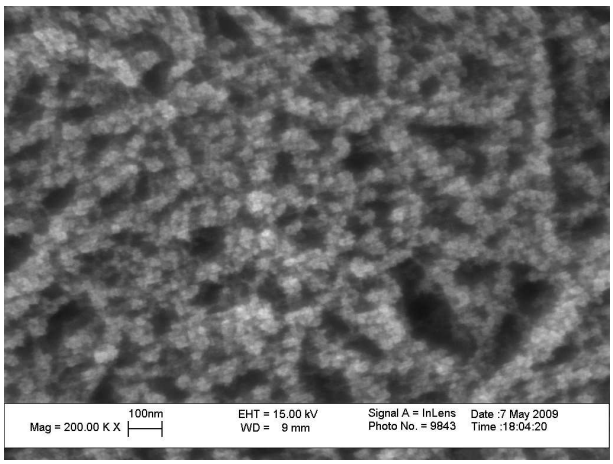

(b)

Figure 4.27: FEG-SEM image of SWCNT bundles distributed over the substrate surface after a 30-min CVD treatment (a) and a higher magnification image of the same deposit (b).

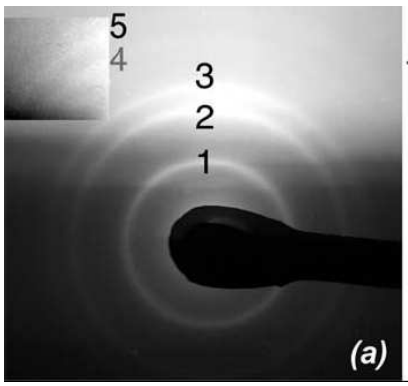

	d_{hkl}	d_{sp}(Å)
1	111	2.06
2	220	1.26
3	311	1.07
4	400	0.89
5	331	0.82

(b)

Figure 4.28: (a) RHEED pattern of samples obtained from a deposition process.(b) Indexing (d_{hkl}) and interplanar distances (d_{hkl} corresponding to the various rings, as labeled in the pattern.

It is worth noticing the absence of the ring corresponding to the forbidden diffraction (220) that usually characterizes the diffraction patterns of polycrystalline diamond materials [48]. It can be explained with a double diffraction phenomenon, the occurring of which requires crystalline grains relatively large (at least some tens of nm).

In our case, the extremely reduced sizes of our diamond crystallites (typically, of the order of 10 nm or less, according to SEM images reported in Fig. 4.27) probably inhibit the double diffraction effect.

Raman spectra of the sample recorded before and after the diamond deposition exhibited very similar features both in the radial breath modes (**RBM**) region and in the D and G bands region, suggesting that the CVD process did not modify the SWCNT structure, as it can be observed in Fig. 4.29.

The Raman signal of the nanodiamond phase was not detected, likely because of the surface hydrogenation of the CVD-grown diamond [49].

As the current focus of this research is on integrating these hybrid materials into a wide range of application fields, among them field emission based devices is the most appealing nowadays, a functional characterization, as field emission cathodes, has been tested for the as synthesised material.

The fact that the diamond surfaces do not adsorb chemical species makes it possible to use the emitters without the need of the initial 'conditioning' procedure, consisting in complex outgassing steps, as required in the case of uncoated CNTs [50, 51].

Moreover, it has been recently demonstrated [48] that in case of nanodiamond films the unavoidable nondiamond carbon contents is the key factor to permit an easy electron

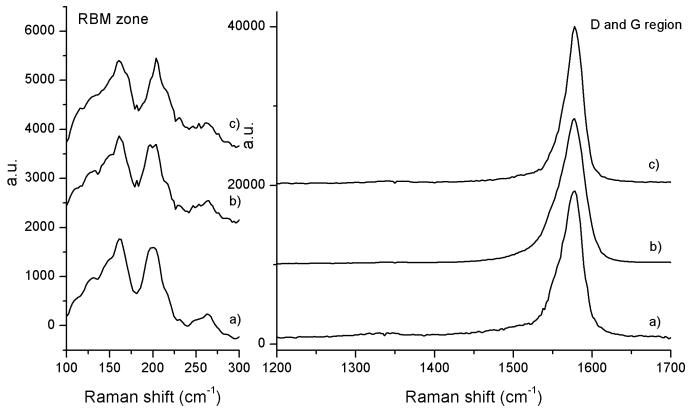

Figure 4.29: Raman spectrum of the CNT bundles before (a) and after the coating process (b).

conduction from back to front surface.

The FE measurements have been carried out at room temperature and working pressure of 10^{-8} mbar, using as anode a Mo sphere with a diameter of 1.00±0.05 mm. All the samples have been tested at a fixed anode-cathode distance of 200 μm, determined by a capacitive approach using an LRC meter (Stanford Research SR715 model).

The FE data obtained in a sphere to plane diode geometry were analysed in the frame of *Fowler-Nordheim* model [34] using the same analytical approach described in ref 21.

Previous works, related to the process of field emission from CNT-based cathodes, have stressed the need of a preconditioning step, carried out by the application of a moderate electric field, to stabilize the emission [51, 50].

The outgassing of loosely bound adsorbates from the emitters surfaces and the rearrangements of the strongly bound ones in a stable energetic configuration concur reasonably well to stabilize the structure of the emitters, the work function ($\phi value$) and consequently the emission properties [52].

Conversely, in the case of the nanodiamond/SWCNT systems, many I/V sweeps performed during the data acquisition sessions have evidenced a stable and reproducible current emission, even from the very beginning, without the need of any preconditioning procedure.

In Fig. 4.30, we show the trend of the emitted current versus time at 1000, 1500, and 1800 V constant voltages. In our prolonged (up to 24 h) emission sessions, differently

from other experiments [51, 50] no relevant discharges or spikes due to emitted adsorbates have been produced and the emitted current remained constant and stable over time.

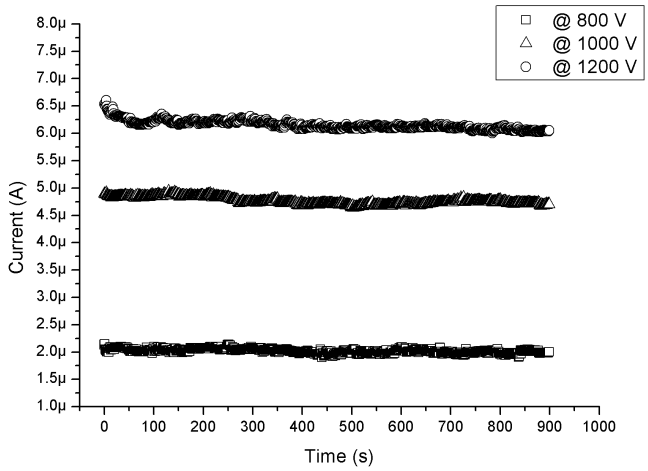

Figure 4.30: Test of stability of current emission vs time at three different values of applied voltage: 800, 1000, and 1200 V.

Figure 4.31 shows the emitted currents as a function of the applied voltage in the range 400–1300 V with an incremental step of 50V for three consecutive experimental runs. Even after several voltage sweeps the I-V curves did not show a relevant drift.

From the recorded data, the turn-on field is 1.7 V/μm. From experimental data, using the analytical approach described in [53] the current density J (at E =6.2 V/μm) was 6 mA/cm^2, being the geometrical enhancement factor β about 1500.

The emission features of the nanotube/nanodiamond material could be rationalized, at a first level of approximation, by considering an emission model fundamentally based on the presence of a layered system characterized by a Csp^2-Csp^3 interface and by a surface-vacuum border [54].

In the framework of such a model the electrons, originated in the sp^2 carbon, are expected to tunnel from the CNT emitters into the conduction band of diamond and to be drifted over the H-terminated diamond surface, with low or negative electron affinity, to the vacuum level.

The emission would result therefore strongly affected by band bending causing a more efficient tunnelling and a lowering of the work function. With respect to the dielectric materials, diamond is expected to give the best results [55]. However, our FE results revealed only a little variation of the emitting properties in comparison with the typical

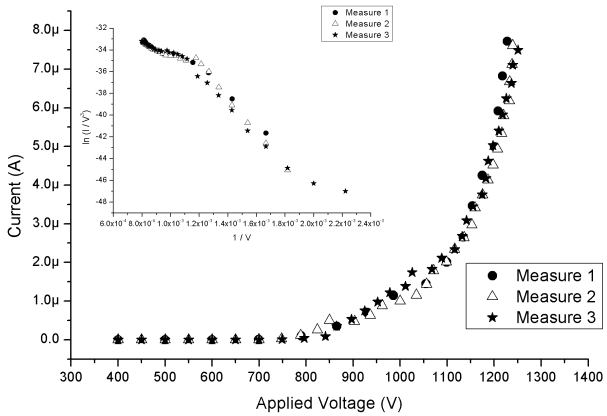

Figure 4.31: Emitted current vs applied voltage measured during three runs from the nanodiamond-coated SWCNT. In the inset plots of the Fowler–Nordheim type are shown.

uncoated nanotube samples prepared following the same methodology.

This seems to indicate only a *'passive effect'* of diamond coating on nanotubes. In fact the improvement of emission properties, due to the presence of wide band gap materials (WBGMs) as in the case of crystals of nanodiamond, is strongly related to the optimization of coating thickness. In particular, in our case the coating is not in form of uniform layer but in form of nanometric particles and, as a consequence, the emission properties depend on their shape, dimension, and texturing.

Moreover the presence of nondiamond carbon species, mainly located at the grain boundaries of the nanocrystalline deposit could mask the improving role of nanodiamond coating creating electron traps [56]. In fact the electrons, originating from CNT bundles, could tunnel through both diamond nanocrystals and grain boundaries consisting of sp^2 carbon phases.

In particular, the grain boundaries can influence the emission properties of micro e nanostructured diamond films. For these systems the grains boundaries can be described as a triple junction (diamond-graphite-vacuum). Here the emission may be facilitated, because the electrons emitted from the graphite located at the grain boundary experiment a diamond work function whose values, in the case of hydrogenated diamond surface, range between 4.2 and 3 eV [57, 58].

This improving effect is true only for controlled graphite amount in the film (lower

than 80%) and when the graphite grains sizes are less than 4 nm. For a quasi total graphite film or for larger graphite patches (grains sizes >4 nm) on surface, the work function value practically clashes with the graphite one.

5 Conclusions

This three year work dealt with the synthesis and characterizations of nanodiamond-based materials and hybrid Csp^2-Csp^3 systems.

The task to assemble three-dimensional networks of closely packed diamond nanograins with predefined shapes, and to use them as substrates for diamond CVD, has been faced aiming at the scientific findings but also at the development of production technologies for diamond-on-diamond devices. With this aim, in particular in a first part of the experimental work we have optimized the synthesis conditions to obtain CVD polycrystalline diamond films by using a colloid of detonation nanodiamonds particles which showed an interesting surface-assisted self-assembling process.

We have produced *'shaped'* polycrystalline diamond films with exotic architectures as 'star-like'or polyhedral structures and self-standing micrometric tips. From the structural characterizations it has been possible to evaluate a good crystallographic quality (by means of Raman spectroscopy, x-ray and electron diffraction) and the presence of a preferred orientation of growth for the CVD diamond coating in function of the colloid fraction used for the seeding process on the substrate.

The use of DND aggregates coupled with CVD-grown diamond layers represents a way in which diamond components can be fabricated into net shapes for MEMS/NEMS applications, tip arrays or junctions for electronic devices. The results obtained have been discussed in Ref. [59]

Until now, diamond has been nucleated and grown on diamond itself, plus a large variety of non-diamond substrates, including metals, semiconductors, insulators, graphite, and even fused glass. But diamond nucleation on the substrate surface critically depends on the, chemical nature and surface condition of the deposition substrate.

Starting from these considerations, in this work of thesis the CVD synthesis of polycrystalline diamond films onto an innovative substrate with superconductive properties, as niobium nitride (NbN), has been investigated. In particular we have studied the catalytic effect deriving from the nature of surface substrate on the diamond growth

by performing CVD syntheses on patterned NbN/Si substrate without any substrate pretreatment and for different runs of deposition.

From the preliminary results obtained under predefinite experimental conditions we have observed, from the early step of synthesis (after 10 minutes), that there is the formation of a larger number of nuclei on the NbN surface than on the Si substrate (the nuclei density value calculated for NbN substrate is approximatively twice that for Si substrate). Moreover the growth rate of diamond on NbN surface is higher than on the Si substrate.

At the same time, we have also evidenced as the NbN layer endured under the drastic conditions of synthesis (strong H_2 etching process), by XRD measurements and this last result is of great importance under a possible future application of diamond films on NbN within electronic devices.

Starting from these results we have carried out CVD diamond synthesis onto a patterned substrate made as a $Si/SiO_2/NbN$ interdigitated electrodes of a multifinger device. From the deposit produced after, at lest, 1 hour of CVD synthesis we have observed, from SEM characterizations, that diamond growth is faster along the NbN patterned electrodes than on the SiO_2 areas. Moreover the polycrystalline films are composed of grains with well defined shape.

More recently, an important task is represented by the study of the benefits obtained by the integration of different nanosized carbon forms to produce novel hybrid Csp^2-Csp^3 systems. These systems, composed by CNT and diamond, can be expected to have unique mechanical properties, excellent electrical and thermal conductivities and field emission characteristics comparable to or better than pure diamond and CNTs.

With this aim, an important part of this work reported the preliminary results obtained with a one-step synthesis, by means of the CVD technique, of CNTs/nanodiamond systems and their structural, morphological and functional characterizations. Already in a previous work [4], our group employing a modified HFCVD set-up capable of delivering nanocarbon particles to the reaction region, used Si samples pre-coated with submicron Fe clusters to obtain nanocrystalline diamond coated bundles of CNTs. In particular these strategies provided the study and application of experimental parameters usually adopted for the CVD growth of CNTs and diamond in a sort of *'mixed way'*.

Particularly, the experimental line followed dealt with a first step in which we have used the typical synthesis conditions for diamond growth in presence, at the same time, of metal catalyst and high substrate temperature while in the second the CNTs growth

parameters have been adopted in absence of the catalyst and with low substrate temperature.

From the preliminary results obtained with these two synthesis approaches we have confirmed that by using the synthesis conditions for the diamond growth but in presence of the metal catalyst and high substrate temperature, the deposit obtained was formed mainly from Csp^2 structures with a high defect degree (as confirmed by Raman spectrum also) which produce sheet-like structures. On the other hand by using the typical CNTs growth conditions in absence of metal catalyst and with a low substrate temperature a diamond ball-like deposit was produced, confirming that none of the two previous steps exploited are able to produce CNT/nanodiamond hybrids.

As consequence of these results the next CVD growths have been carried out using CNTs as template for the CVD diamond growth. In particular in a first case we have preliminarily synthesized SWCNTs with our HFCVD apparatus and then applied the conditions to nucleate and grow diamond onto the CNT template for run from 30 minutes to 3 hours. From the SEM images, it is clear the presence of the hybrid system constituted by the CNTs and nanocrystalline diamonds. Moreover the presence of the crystals with nanometric dimensions located most of all on surface of some CNTs bundles and a large area of CNTs deposit coated by diamond crystals with well shaped facets and with dimensions under 500 nm can be evidenced.

In alternative, in this contest we have explored another preparation route of hybrid CNT/nanodiamond structures, suitable to be scaled up and adapted to the requirements of electronic industries. The coating by CVD of commercial single wall carbon nanotubes with crystalline diamond nanoparticles have been reported. For further information see Ref. [60].

The samples produced have been analysed by means of morphological-structural techniques (SEM, Raman spectroscopy, RHEED) and also tested as field emission cold cathode with our FE apparatus. The results obtained confirmed the presence of nanocrystalline diamond on the side wall of the SWCNTs. Moreover if we compared the the coating obtained with these last conditions and those reported above we can suppose that the decoration of commercial CNTs follows a sort of instantaneous nucleation (in which all the nuclei are produced and then ready to grow).

Instead in the case of diamond on CNTs prepared in our laboratory, the growth follows a sort of 'progressive nucleation' (in which a progressive formation of nuclei is observed and then increased). This fact may be rationalized by considering the differences in

defectivity of the two kind of CNTs and it is a clear indication of the fundamental role played by the structure of carbon surfaces in the process of diamond synthesis.

From the applied point of view, we have addressed the task of realizing efficient and robust SWCNT-based cold cathodes produced by depositing nanocrystalline diamond on bundles mats of SWCNT that, after the coating process, still retain their pristine structure. Differently from the uncoated CNTs and from other nanocarbons, no conditioning procedures are needed at the beginning of the process in order to stabilize the emission. This last characteristics is a key point for applications that require short time response of the emitter.

Overall the good emission behaviour, coupled with the relevant mechanical resistance and the chemical properties conferred by the outermost diamond coating, makes the cold cathodes assembled with SWCNT/nanodiamond suitable for applications in harsh and radiation hard environments. Envisaged applications for such robust electron sources include industrial welders and space operations (thrusters, tethers), but also the use as injectors in plasma reactors and electroncyclotron-resonance ion sources.

6 List of publications

Papers

- M.L. Terranova, S. Orlanducci, E. Tamburri, V. Guglielmotti, F. Toschi, D. Hampai, M. Rossi, *'Polycrystalline diamond on self-assembled detonation nanodiamond: a viable route for fabrication of all-diamond preformed microcomponents'*, Nanotechnology, **19**, 415601, (2008)

- Z.D. Kovalyuk, F.V. Motsnyi, O.S. Zinets, S.P. Yurcenyuk, E. Tamburri, S. Orlanducci, V. Guglielmotti, M.L. Terranova, F. Toschi, M. Rossi , *'An innovative and viable route for the realization of ultra-thin supercapacitors electrodes assembled with carbon nanotubes'*, Journal of Nanoscience and Nanotechnology, **9**, 2124, (2009)

- E. Tamburri, F. Toschi, V. Guglielmotti, E. Scatena, S. Orlanducci, M.L. Terranova,), *'Nanofabrication by Electrochemical Routes of Ni-Coated Ordered Arrays of Carbon Nanotubes'*, Journal of Nanoparticle Research, **11**, 1311, (2009)

- V. Guglielmotti, S. Chieppa, S. Orlanducci, E. Tamburri, F. Toschi, M.L. Terranova, M. Rossi, *'CNT/nanodiamond structures: an innovative concept for stable and ready-to start electron emitters'*, Applied Physics Letters, **95**, 222113, (2009) (also selected for: Virtual Journal of Nanoscale Science and Techonolgy)

- D. Hampai, S. B. Dabagov, G. Cappuccio, A. Longoni, T. Frizzi, G. Cibin, V. Guglielmotti, M. Sala, *'Elemental Mapping and Micro-Imaging by X-Ray Capillary Optics'*, Optics Letters, **33**, 2743, (2009)

- M.L. Terranova, V. Guglielmotti, S. Orlanducci, V. Sessa, E. Tamburri, M. Rossi, *'Preparation and functional characterizations of Ta_2O_5 deposits organized at the nanoscale'*, ECS Transactions, **25**, issue 8, 1153, (2009)

Proceedings

- D. Hampai, S.B. Dabagov, G. Cappuccio, A. Longoni, T. Frizzi, G. Cibin, V. Guglielmotti, M. Sala, V. Sessa, *'X-ray microfocusing by polycapillary optics'*, Proc. SPIE, **7077**, 70770U, (2008)

- F. Toschi, E. Tamburri, V. Guglielmotti, M.L. Terranova, A. Reale, A. Di Carlo, D. Passeri, M. Rossi, C. Falessi, A. Fiorello, R. Buttiglione, *'Preparation and thermal characterization of carbon nanotube-based composites for applications in electronic packaging*, Proc IEEE - IARIA Conf ICQNM 2008 - The Second International Conference on Quantum, Nano, and Micro Technologies - Sainte Luce, Martinique, 55,(2008)

Ringraziamenti

Desidero innanzitutto ringraziare Antonio per la sua smisurata pazienza nel sopportarmi tutte le sere in cui 'ho fatto tardi' nel tentativo di terminare questo lavoro in tempo utile. Forse avrà perso qualche ora di sonno per colpa mia ma può vantarsi, se vuole, che parte di questi risultati sono anche suoi.

Ovviamente mi è doveroso ringraziare Emanuela e Silvia per l'enorme disponibilità che mi hanno reso nonostante i tempi fossero stretti, qualche malanno girasse nel laboratorio e qualche bambino sonnambulo turbasse la quiete notturna!

Ringrazio anche chi, pur essendo presente durante i miei 'deliri scientifici' si è astenuto dall'aumentare lo stato di ansia che poteva colpirmi negli ultimi giorni di scrittura, ma anzi mi ha 'sedato' con del buon cioccolato.

Come non ringraziare il mio 'fidato socio' Dariush per avermi re-introdotto di nuovo nel mondo di Latex nonostante avessi rimosso ogni ricordo sul suo utilizzo: grazie per avermi spronato soprattutto all'inizio quando lo scoramento causato dai numerosi messaggi di Warning e Error mi aveva fatto preda!

Infine, ma non per questo di minore importanza, ringrazio la Prof. Maria Letizia Terranova per i numerosi 'pungoli' scientifici che ogni giorno ci regala e che diventano spesso fonte di interessanti discussioni (forse altre volte solo voli pindarici), nonchè per la sua estrema disponibilità e gentilezza nei confronti di chiunque lavori al suo fianco.

Forse dimenticherò qualcuno ma considerando come ho trascorso le ultime nottate direi che merito un 'condono' per tutte le mie dimenticanze.

Bibliography

[1] E. Butler, and A. V. Sumant, *Chem. Vap. Dep.* **14**, 145 (2008).

[2] Q. Yang, S. Yang, C. Xiao, and A. Hirose, *Mater. Lett.* **61**, 2208 (2007).

[3] L. T. Sun, J. L. Gong, Z. Y. Zhu, D. Z. Zhu, S. X. He, Z. X. Wang, Y. Chen, and G. Hu, *Appl. Phys.Lett.* **84**, 2901 (2004).

[4] M. Terranova, S. Orlanducci, A. Fiori, E. Tamburri, and V. Sessa, *Chem. Mater.* **17**, 3214 (2005).

[5] X. Xiao, J. W. Elam, S. Trasobares, O. Auciello, and J. A. Carlisle, *Adv. Mater.* **17**, 1496 (2005).

[6] N. S. Xu, and S. E. Huq, *Mater. Sci. and Eng.* **R48**, 47 (2005).

[7] J. B. Cui, J. Ristein, and L. Ley, *Phis. Rev. Lett.* **81**, 429 (1998).

[8] M. Werener, and R. Locher, *Rep. Prog. Phys.* **61**, 1665 (1998).

[9] S. Koizumi, M. Kamo, Y. Sato, M. Mita, A. Sawabe, A. Reznick, S. Uzan-Saguy, and R. Kalish, *Dia. Relat. Mat.* **7**, 540 (1998).

[10] S. Orlanducci, *Materiali compositi e nanostrutturati a base carbonio: sintesi, caratterizzazione ed applicazioni*, University of Rome Tor Vergata, 2000.

[11] M. Baidakova, and A. Y. Vul', *J. Phys. D: Appl. Phys.* **40**, 6300 (2007).

[12] A. Y. Vul', V. Y.Dolmatov, D. M. Gruen, and O. Shenderova, *Detonation nanodiamonds and related materials*, Bibliography Index 2nd issue, St Petersburg: Ioffe Physico-Technical Institute, 2006.

[13] V. V. Danilenko, *Synthesis, Properties and Applications of Ultrananocrystalline Diamond*, D. Gruen et al, 2005, p. 181.

[14] M. H. Amin, A. A. Mottalebizadeh, and S. Borji, *Dia. Relat. Mater* **18**, 611 (2009).

[15] B. Palosz, C. Pantea, E. Grzanka, S. Shelmakh, T. Proffen, T. W. Zerda, and W. Palosz, *Dia. Relat. Mater* **15**, 1813 (2006).

[16] T. Dideykin, E. D. Edeilman, and A. Y. Vul', *Solid State Commun.* **126**, 495 (2003).

[17] P. K. Bachmann, H. J. Hagemann, H. Lade, D. Leers, F. Picht, D. U. Weichert, and H. Wilson, *Mater. Res. Soc. Symp. Proc.* **339**, 267 (1994).

[18] E. Molinari, R. Polini, V. Sessa, M. Terranova, and M. Tomellini, *J. Mater. Res.* **8**, 785 (1993).

[19] P. K. Bachmann, H. J. Hagemanna, H. Lade, D. Leers, F. Picht, D. U. Weichert, and H. Wilson, *Mater. Res. Soc. Symp. Proc.* **339**, 267 (1994).

[20] D. Goodwin, and J. Butler, *Handbook of Industrial Diamonds and Diamond Films*, Marcel Dekker, New York, 1998, vol. 57, p. 11.

[21] C. Wild, R. Kohl, N. Herres, W. Müller-Sebert, and P. Kooid, *Dia. Relat. Mater.* **3**, 373 (1994).

[22] P. M. Menon, R. E. Clausing, L. Heatherly, and C. S. Feigerle, *Dia. Relat. Mater.* **7**, 1201 (1998).

[23] H. Liu, and D. S. Dandy, *Dia. Relat. Mater.* **4**, 1173 (1995).

[24] M. S. Dresselhaus, G. Dresselhaus, and R. Saito, *Physical properties of carbon nanotubes*, Imperial College Press London, 1998.

[25] A. Thess, *Science* **273**, 483 (1996).

[26] S. Ijima, *Nature* **354**, 56 (1991).

[27] M. L. Terranova, V. Sessa, and M. Rossi, *Chem. Vap. Dep.* **12**, 315 (2006).

[28] J. T. Drotar, B. Q. Wei, G. R. Y. P. Zhao and, P. M. Ajayan, T. M. Lu, and G. C. Wang, *Phys. Rev. B* **64**, 125417 (2001).

[29] Q. Yang, C. Xiao, W. Chen, and A. Hirose, *Dia. Relat. Mater.* **13**, 433 (2004).

[30] N. Shankar, N. G. Glumac, M. Yu, and S. Vanka, *Diam. Relat. Mater.* **17**, 79 (2008).

[31] A. J. S. Fernandes, M. Pinto, M. A. Neto, F. Oliveira, R. Silva, and F. M. Costa, *Dia. Relat. Mater.* **18**, 160 (2009).

[32] A. Einstein, *Annalen der Physik* **17**, 132 (1905).

[33] O. W. Richardson, *Phil. Mag.* **28**, 633 (1914).

[34] H. Fowler, and L. W. Nordheim, *Proc. R. Soc. Lond. Ser. A* **119**, 173 (1928).

[35] M. V. Badakova, A. Y. Vul', V. G. Golubev, S. A. Grundikin, V. G. Melekhin, N. A. Feoktistov, and A. Krueger, *Semiconductors* **36**, 615 (2002).

[36] J. Phillip, P.Hess, T. Feygelson, J. E. Butler, S. Chattopadhyay, K. H. Chen, and L. C.Chen, *J. Appl. Phys.* **93**, 2164 (2003).

[37] I. Larionova, V. Kuznetsov, A. Frelov, O. Shenderova, S. Moseenkov, and I. Mazov, *Dia. Relat. Mater.* **15**, 1804 (2006).

[38] E. Osawa, *Dia. Relat. Mater.* **16**, 2018 (2007).

[39] I. Kulacova, *Phys. Sol. State* **46**, 636 (2004).

[40] Z. Zhu, *Mod. Phys. Lett. B* **17**, 1477 (2003).

[41] A. V. Oktrub, L. G. Bulusheva, I. S. Larionova, V. L. Kuznetsov, and S. L. Molodtsov, *Dia. Relat. Mater.* **16**, 2090 (2007).

[42] M. H. Grimsditch, E. Anastassakis, and M. Cardona, *Phys. Rev. B* **18**, 901 (1978).

[43] J. W. A. III, and M. D. Drory, *Phys. Rev. B* **48**, 2601 (1993).

[44] H. Windischmann, G. F. Epps, Y. Cong, and R. W. Collins, *J. Appl. Phys.* **69**, 2231 (1991).

[45] W. Wang, K. Liao, J. Gao, and A. Liu, *Thin Solid Films* **215**, 174 (1992).

[46] A. Ferrari, and J. Robertson, *Phys. Rev. B* **61**, 14095 (2000).

[47] M. Dresselhaus, G. Dresselhaus, A. Jorio, A. S. Filho, and R. Saito, *Carbon* **40**, 2043 (2002).

[48] M. Rossi, G. Vitali, M. L. Terranova, and V. Sessa, *Appl. Phys. Lett.* **63**, 2765 (1993).

[49] E. Maillard-Schaller, O. M. Kuettel, L. Diederich, L. Schlapbach, V. V. Zhirnov, and P. I. Belobrov, *Dia. Relat. Mater.* **8**, 805 (1999).

[50] A. Dean, and B. R. Chalamala, *Appl. Phys. Lett.* **76**, 375 (2000).

[51] C. Dong, and M. C. Gupta, *Appl. Phys. Lett.* **83**, 159 (2003).

[52] V. Semet, V. T. Binh, P. Vincent, D. Guillot, K. B. K. Teo, M. Chhowalla, G. A. J. Amaratunga, W. I. Milne, P. Legagneux, and D. Pribat, *Appl. Phys. Lett.* **81**, 343 (2002).

[53] I. Boscolo, A. F. S. Cialdi and, S. Orlanducci, V. Sessa, M. L. Terranova, A. Ciorba, and M. Rossi, *J. Vac. Sci. Technol. B* **25**, 1253 (2007).

[54] W. B. C. J. J. C. V. V. Zhirnov, G. J. Wojak, and J. J. Hren, *J. Vac. Sci. Technol. A* **15**, 1733 (1997).

[55] Z. Wang, B. Wang, H. Wang, H. Zhou, A. P. Huang, M. K. Zhu, H. Yana, and X. H. Yan, *Appl. Phys. Lett.* **81**, 2782 (2002).

[56] D. Pradhan, and I. N. Lin, *Appl. Mater. Interfaces* **1**, 1444 (2009).

[57] J. B. Cui, and J. Robertson, *J. Vac. Sci. Technol. B* **20**, 238 (2002).

[58] B. Cui, M. Stammler, J. Ristein, and L. Ley, *J. Appl. Phys.* **88**, 3667 (2000).

[59] M. L. Terranova, S. Orlanducci, E. Tamburri, V. Guglielmotti, F. Toschi, D. Hampai, and M. Rossi, *Nanotechnology* **19**, 415601 (2008).

[60] V. Guglielmotti, S. Chieppa, S. Orlanducci, E. Tamburri, F. Toschi, M. L. Terranova, and M. Rossi, *Appl. Phys. Lett.* **95**, 222113 (2009).